THERMAL PERFORMANCE OF METALLIC NANOFLUIDS IN MICROCHANNEL HEAT SINK

Duncan Clark

Engineering (Honours with a stream in Mechanical Engineering)

Department of Mechanical Engineering
Macquarie University

November 6, 2017

Supervisor: Dr. Ann Lee

ACKNOWLEDGMENTS

I would like to acknowledge the help of my academic supervisor Dr. Ann Lee with the guidance he has shown me to understand the required information needed to work on this project. The support of my girlfriend Mirei as an ear to listen to various obsticals encountered during the thesis is greatly appreciated as it helped me make choices envolved in the simulation process. I would also like to thank the Macquarie University Engineering Department for giving me access to the necessary programs and learning spaces used throughout this thesis project.

STATEMENT OF CANDIDATE

I, Duncan Clark, declare that this report, submitted as part of the requirement for the award of Bachelor of Engineering in the Department of Engineering, Macquarie University, is entirely my own work unless otherwise referenced or acknowledged. This document has not been submitted for qualification or assessment and any academic institution.

Student's Name: Duncan Clark

Student's Signature: D.C. Clark

Date: 6, Nov, 2017

ABSTRACT

A Numerical investigation of the heat transfer enhancement of a two-dimensional microchannel heat sink (MCHS) using Al_2O_3-water, CuO-water and TiO_2-water was conducted. The numerical methodology uses mathematical models for continuity, momentum, energy and solid temperature to model the fluid flow through the MCHS. The effect of the metallic nanoparticles on the thermal performance of the heat transfer fluid (HTF) in the heat sink was examined for the volume concentrations of 1%, 3%, and 5%. Techniques for increasing the thermal performance of a HTF are to raise the thermal conductivity of the fluid and/or to reduce the viscosity. Analysis on the affect the individual thermo-phyiscal properties have on the thermal boundary layer and the total thermal performance is conducted. The results depict that for Al_2O_3-water and CuO-water nanofluids the overall thermal performance is increased compared to the pure base fluid of water, with the most effective volume concentration at 5% and 3%. TiO_2-water nanofluid decreased in thermal performance at all volume concentrations. Overall, Al_2O_3-water nanofluid at the volume concentration of 5% shows the most effective heat transfer capabilites in the MCHS.

Contents

List of Figures

List of Tables

Chapter 1

Introduction

With the ever increasing global need for smaller more powerful electronic devices, researchers have estimated that the physical limits of Moores law of computing will be reached in the next 20 years [3]. Increasing the density of transistors in microchips leads to difficulties in heat removal that can damage and reduce reliability in the component. To expand the theoretical limits of computing, mechanical engineers have been implementing many advanced methods for heat dissipation in microchips [4]. This has led to development of alternative heat transfer fluids that perform more effectively in heat sinks and that can be manufactured at a lower cost [5].

An example of a new approach to cooling microchips that has had continued development in recent years is the implementation of nanofluids [5]. Nanofluids are the suspension of nanoparticles of diameter 1-100 nm in a base fluid, such as water. The advantages gained from adding metallic particles to a pure fluid are most clearly gained on the nanometer scale [6]. Experiments done on larger scale particles in the micrometre and millimetre range have shown severe problems with abrasion and clogging [7]. Nanoparticles also have a higher relative surface area that positively increases the heat transfer capabilities of the particles themselves.

The purpose of this paper is to numerically study the effectiveness of nanofluids Al_2O_3-water, CuO-water, and TiO_2-water in a MCHS. Analysis of the thermal performance of each nanofluid is done to determine the most effective volume concentration of each nanofluid as a HTF in the MCHS. This chapter provides an introduction to nanofluids and an overview of the objectives of this project.

1.1 Nanofluids

Nanofluids is a promising branch of research for mechanical engineering as it theoretically and experimentally shows improvements in heat transfer rates at optimal volume percentages. This proposed alternative of a heat transfer fluid is manufactured by suspending nanoparticles in a base fluid. These nanofluids can be combinations of nanoparticles such as Al_2O_3-water, CuO-water, and TiO_2-water. The thermal properties of the nanoparticles

are carried into the heat transfer fluids to influence the overall efficiency of the thermal performance compared to the pure water.

The effectiveness of HTFs on the heat transfer rate of the heat sink are reliant on the density, heat capacity, thermal conductivity, and the viscosity. While the implementation of the nanoparticles increase the thermal conductivity of the fluid, due to using highly conductive nanoparticles, they also negatively impact the viscosity. This relationship between conductivity and viscosity is related to the volume concentration of the nanofluid. Preliminary experimental results show that increases of thermal conductivity of up to 60% can be achieved through a nanofluid comprised of 5% volume percentage CuO nanoparticles to water [8].

Preparation and maintenance of the nanofluids is an important consideration when implementing a nanofluid cooling system. This is due to changes in the properties of the nanofluid when the nanoparticles are allowed to collect and clump together. The nanofluid does not simply refer to a traditional liquid-solid mixture as some special requirements are necessary to maintain the specific volume percentage and nanoparticle suspension. In general, to maintain the consistancy and stability of the nanofluid the pH levels of the fluid need to be maintained to inhibit any chemical changes in the water, surface activators and/or dispersants are used to break up clusters formed on liquid to solid surfaces, and the use of ultrasonic vibrations to break up any clusters that form during flow of the fluid [8]. These methods ensure that the nanofluid remains stable and the thermal properties will remain consistent. Since this project is using homogeneous nanofluids with properties calculated through various methods based on theoretical and experimental studies though the volume percentages, the required maintenance opperations for suspension are not included in the study.

1.2 Project Overview

This project overview describes the whole project and outlines the processes taken to describe the numerical methodology and to calculate the thermo-physical properties to then simulate an environment to determine the thermal performance of the nanofluid. This project is supervised by Dr. Ann Lee, in the department of Engineering, Macquarie University. Weekly meetings have been organised during consultation hours on Thursday afternoons from 2:30pm-4:00pm to update and help guide the development of this project and any problems encountered in the simulation program. These meetings are to ensure that the research done for this project follows the project plan and that the results of the numerical simulations are correct.

The outline of this thesis are as follows:

- Chapter 2 contains a literature review of the related background theory to this project. Topics discussed are results from similar research papers, physical mechanism accounting for the thermal conductivity enhancement of the nanofluid, Maxwell

equations considered for very dilute suspension of spherical particles, and extensions to the Maxwell equations approximations of thermal conductivity. The methodology used to calculate viscosity using the GMDH method are introduced and the Reynolds number of the fluid in the microchannel heat sink is calculated to determine inlet pressure conditions.

- Chapter 3 contains the governing equations used for continuity, momentum, energy and solid temperature to simulate the fluid flow through the MCHS and the thermophysical property equations used for density, heat capacity, thermal conductivity, and viscosity.
- Chapter 4 provides information about the model dimensions and the meshing approach used to accurately simulate the MCHS.
- Chapter 5 contains the information on the process of verifiying a numerical simulation and how the meshing and calculation methodology used for the microchannel model follow the verification process.
- Chapter 6 depicts results on how the density and heat capacity affect the fluid flow and the overall thermal performance of the nanofluids.
- Chapter 7 depicts the influence viscosity has on the velocity, thermal boundary layers and the overall thermal performance of the nanofluids.
- Chapter 8 depicts the influence thermal conductivity has on the thermal boundary layers and thermal performace of the nanofluids.
- Chapter 9 contains the discussion of the results gathered from the numerical method of simulating the MCHS and the conclusions drawn from this project, as well as, the choice of nanofluid that can be used as an alternative to water as a HTF in a MCHS. An evaluatation of future work that can be done in the numerical study of nanofluids when used as HTFs in MCHSs.
- Chapter 10 is the list of abbreviations and the nomenclature.

1.2.1 Project Objectives

The goals for this project are to investigate the effect nanoparticles have on the thermal performance of a HTF used in the application of a MCHS. An assesment of the feasibility of nanofluids is done by numerically determining the thermal performance of three metal based nanofluids Al_2O_3-water, CuO-water, and TiO_2-water to determine if any volume concentration should be considered an alternative to water as a HTF. This report aims to eliminate the use of inefficient liquids in microchannel cooling by demonstrating more effective alternatives. The process of studying the nanofluids requires a number of stages to be completed:

1. Study exsisting literature on the current applications of nanofluids and other advancements related to cheap heat transfer fluid alternatives.
2. Familiarise with ANSYS modelling, meshing, and Fluent calculation methods to best tailor the calculations to the microchannel heat sink.
3. Create a microchannel heat sink model and develope a meshing that accurately encapsulates the most important features of the model.
4. Use theory in the field of nanofluids to comprise a thermo-physical property table for Al_2O_3-water, CuO-water, and TiO_2-water nanofluids at the volume concetrations of 1%, 3%, and 5%.
5. Verify the residuals conditions for the simulation calculations using the default water properties.
6. Run numerical simulations on each individual set of thermo-physical properties and comprise results for temperature of the bottom surface of the silicon in the microchannel, velocity profile in the microchannel and a temperature contour to use in the results and discussion sections of this report.
7. Analyse the impact the individual thermo-physical properties have on the overall thermal performance of the nanofluids.
8. Discuss the relationship between the thermo-physical properties to the thermal boundary layers and thermal performance to determine the most effective concentration for each of the numerically simulated nanofluids.
9. Discuss the results of the numerical simulations and describe features of the results and explain how they relate to the thermo-physical properties. Determine the applicability of the nanofluids as an alternative to water as a heat trasnfer fluid in a microchannel heat sink.
10. Conclude the results of which nanofluids can be considered as viable alternatives to heat transfer fluids in the microchannel heat sink application.
11. Recommend future areas of work in the field of nanofluids.

1.3 Baseline Review

This project began on 21st of August 2017 and is to be concluded on the 6th of November 2017. The project plan has included all dates between the beginnings of the project to the end of the project as available for project activities. Dates that project work has been completed have been documented in the form of a logbook that has been recorded since the start date of the project.

Chapter 2

Literature Review

2.1 Nanofluids HTF Application

Many industrial processes involve a heat exchange whether it be to transport heat to be used on another system or to transfer heat away from a component with a heat sink to protect it from damage. The method of heat transfer also has much variety such as, flowing fluid in either laminar or turbulent regime, as well as, stagnant boiling fluids [6]. Many of the methods used would greatly benefit from having a fluid that has a lower thermal resistivity [6]. Advantages for using highly conductive fluids include, smaller heat transfer systems, improved energy efficiency, lower system cost and maintenance. Nanofluids have the potential to impact thermal performance in the fields of transportation, electronics, medical, food and industrial manufacturing of many types.

The term nanofluids was first used in a report from 1995 titled *Enhancing Thermal Conductivity of Fluids with Nanoparticles* when describing nanoparticles of approximately 10 nm suspended in water, ethylene glycol, and engine oil [6]. The report concluded results based on Maxwell equations that theoretically showed the relationship between nanoparticle sphericity and the conductivity ratio of the copper-water nanofluid.

Since then, many researchers have determined that for many heat transfer fluids a volume concentrations of 0.5-4% nanoparticles enhancement do increase the effectiveness of up to 15-40% [5]. Other reports on the effectiveness of nanofluids as a heat transferring fluid show that Copper Oxide (CuO) nanoparticles suspended in an ethylene glycol containing 0.3 volume percentage of CuO increased the thermal conductivity by 4% [9]. The nanoparticles of CuO were ultrafine at an average size of 10 nm, which the report says was a major contributor to the efficiency of the nanofluid.

Another study that was published in the *Journal of Thermophysics and Heat Transfer* showed enhanced thermal conductivity of both CuO and Al_2O_3 nanoparticles when suspended in distilled water, ethylene glycol, engine oil and vacuum pump fluid. Research published in the *International Journal of Thermal Sciences* showed a relationship between volume percentage of TiO_2 nanoparticles in deionized water and the thermal conductivity of the nanofluid for two sizes of nanoparticles [10] . Other research in the nanofluid field follow this project in determining that the metal based nanofluids of Al_2O_3, CuO, and

TiO_2 suspended in liquid water do increase the thermal conductivity of the HTF for low volume percentages [10].

2.2 Maxwell - Garnett Model

To derive an expression for the effective thermal conductivity of a nanofluid mixture using Maxwell idea a very dilute suspension of spherical particles must be considered while ignoring the interactions the particles have with one another, (i.e. clumping and grouping). For a nanofluid containing identical spherical particles of radius r in a field of temperature T and a temperature gradient G, the steady state-condition can be defined by the Laplace equation.

$$\nabla^2 T(r) = 0 \tag{2.1}$$

By considering a larger spherical container of radius r_o containging all the smaller spherical particles dispersed in the fluid matrix one can calculated the temperature T outside the sphere r_o at a distance of $r > r_o$ in the following two ways (Stratton, 1941; Van Beek, 1967). The first method is to consider the spherical container of r_o to be a completely heterogeneous system with an effective thermal conductivity k_{eff} embedded in a matrix with a thermal conductivity of k_m [1]. The temperature outside the spherical container r_o can therefore be expressed as:

$$T(r) = \left(-1 + \frac{k_{eff} - k_m}{2k_m + k_{eff}} \frac{r_o^3}{r^3} \right) G.r \tag{2.2}$$

This is obtained by solving the Laplace Equation together with the following boundary condition:

$$T(r)|_{r\to\infty} = -G.r \quad T(r)|_{r\to\ r_0^-} = T(r)|_{r\to\ r_0^+} \tag{2.3}$$

$$k_e \frac{\partial T(r)}{\partial r}|_{r\to r_o^-} = k_m \frac{\partial T(r)}{\partial r}|_{r\to r_o^+} \tag{2.4}$$

Second, the temperature T is considered to be generated by all the nanoparticles with thermal conductivity k_p mixed into the base fluid matrix with k_m, and using a similar procedure it can be calculated from the superposition principle as:

$$T(r) = \left(-1 + \frac{k_p - k_m}{2k_m + k_p} \frac{\phi_v r_o^3}{r^3} \right) G.r \tag{2.5}$$

After the manipulation of the above formula the effective thermal conductivity k_{eff} can be calculated using the formula below:

$$k_{eff} = k_m + 3\phi_v \frac{k_p - k_m}{2k_m + k_p - \phi_v(k_p - k_m)} \tag{2.6}$$

After manipulation of the above formula the effective thermal conductivity k_{eff} can be calculated using the formula below:

$$\frac{k_{eff}}{k_m} = \frac{(1-\phi_v)(k_p+2k_m)+3\phi_v k_p}{(1-\phi_v)(k_p+2k_m)+3\phi_v k_m} \tag{2.7}$$

This is the conventional Maxwells - Garnett effective medium self-consistent approximation that has been used to describe the effective thermal conductivity of a two components mixture applied to nanofluids. The Maxwell equation only takes into consideration the volume concentration and the thermal conductivies of the nanoparticle and base fluid and not the interactions between the particles and the base fluid or other individual particles. This is why this expression for effective thermal conductivity has been improved on in several studies to improve the equation to relate to other important factors such as particle size and shape and nanolayers.

The effective thermal conductivity calculated in this study focuses on a simulation rather than an experiment, the effective thermal conductivity are based on fixed assumptions of the homogeneous nanofluid. For example, the size and shape of the nanoparticles play a substantial role in the theorised results so the assumption of perfect spherical shape and regular diameters of 10 nm are taken.

2.3 Improvements on Maxwell's Equations

Maxwells equations describe the effective thermal conductivity of a mixture of two components by relating the volume concentration and the thermal conductivity of the two individual components. For certain cases where the volume concentration is low, nanoparticles hold sufficient spherical shape and where the nanofluid is successfully held in stable suspension this approximation is accurate. However, for the purposes of this project, while assumptions are made to the spherical shape and homogeneous nanoparticle suspension, the nanoparticle volume percentage range from 1-5% so alternative approximations of thermal conductivity are made.

The equations used to approximate the thermal conductivity of the nanofluids in this project are based on studies done by W. Yu and S.U.S Choi [1]. The research done shows how the interfacial layers around the nanoparticles while in suspension effect thermal conductivity on small nanoparticles from 3-15 nm in diameter at concentrations of 1-5%. The below image shows how when suspended in a base fluid, the nanoparticles form a layer of liquid particles around them in a sort of shell which disrupts the simple thermal interaction between the nanoparticles and the liquid.

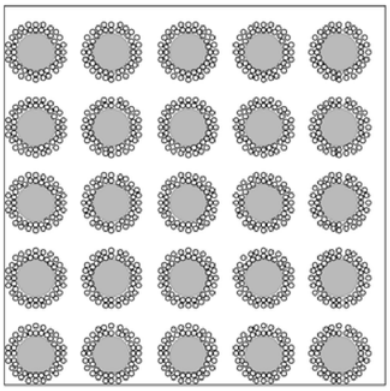

Figure 2.1: Nanolayers of several nanoparticles in a bulk liquid [1]

This layer around the nanoparticles is called a nanolayer and it is believe to be more ordered than the surrounding liquid and therfore has a higher thermal conducitivty compared to the bulk liquid. Because the nanolayer remains attached to the nanoparticle in suspension it can be treated as one particle. To combine the particles an equation needs to be used to alter the volume concentration of the new particle to base liquid [1].

$$\phi_v^{\backslash} = \frac{4}{3}\pi(r+t)^3 n = \frac{4}{3}\pi r^3 n(1+\frac{t}{r})^3 = \phi_v(1+\beta)^3 \tag{2.8}$$

where n is the particle number per volume and $\beta = \frac{t}{r}$ is the ratio of the nanolayer thickness to the original particle radius. To determine the thermal conductivity of the new particle the below equation must be used:

$$k_{pe} = \left(\frac{[2(1-\gamma)+(1+\beta)^3(1+2\gamma)]\gamma}{-(1-\gamma)+(1+\beta)^3(1+2\gamma)}\right)k_p \tag{2.9}$$

where $\gamma = \frac{k_{layer}}{k_{particle}}$ is the ratio of nanolayer thermal conductivity to paticle thermal conductivity, a crucial ratio for this method of effective thermal conductivity calculation. In the extreme case where $k_{layer} = k_{particle}$,(i.e. $\gamma = 1$)the above expression simplifies down to $k_{pe} = k_p$ which means the nanolayer has formed into the nanoparticle and has gained the thermal characteristics of the nanoparticle material which is impossible in this projects experiment. Using the two expressions above we can apply both to the Maxwell equation to get:

$$k_{eff} = \frac{k_{pe}+2k_m+2(k_{pe}-k_m)(1+\beta)^3\phi_v^{\backslash}}{k_{pe}+2k_m-(k_{pe}-k_m)(1+\beta)^3\phi_v^{\backslash}}k_m \tag{2.10}$$

Results from implementing this calculation on copper-oxide-in-ethylene-glycol of particle size ranging from 3-15 nm and nanolayer thickness between 1-2 nm show a thermal

conductivity increase of between 3-8 fold compared to the classic Maxwell model for certain k_{layer} properties. For more realistic values for $k_{layer}(k_{layer} = 10k_1, 100k_1)$ results still show and increased thermal conductivity ratio of between 1.1-1.9 which still shows substantial efficiency increase. Comparisons between the theoretical nanolayer equations and experimental results show that the nanolayer theory more closely matches than the classical Maxwell equations for $k_{layers} = 10k_1, 100k_1$, and k_p [1].

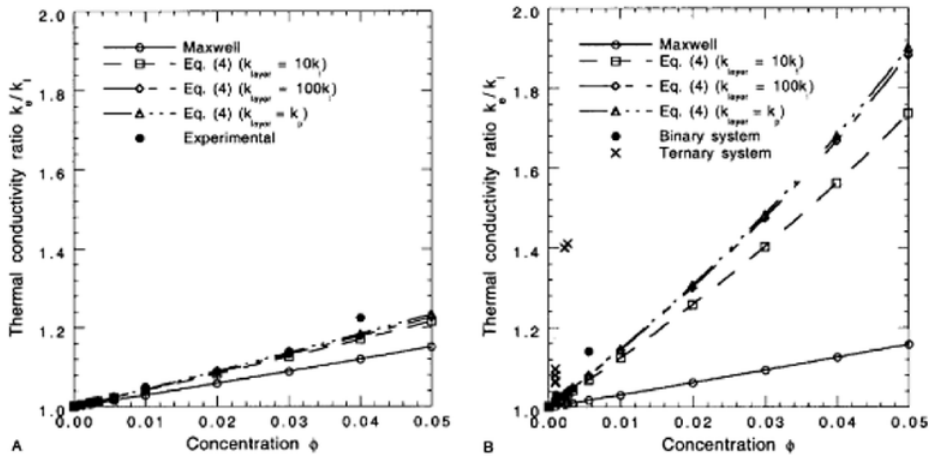

Figure 2.2: Thermal Conductivity ratio vs. nanoparticle concentration for Copperoxide-in-ethylene-glycol for particle of 15 nm (left) and 3 nm (right) [1]

This study concludes that an alternative to using higher volume concentrations >5% for nanofluids is to lower the nanoparticle size to <10nm to gain the added benefits of the nanolayers surrounding the nanoparticles. For this project however, the nanolayer and nanoparticle sizes are fixed while the concentrations of the metallic nanoparticles have varying volume percentages of between 1-5%. The nanolayers are considered to better describe the mechanism that the nanofluids are using to transfer heat along the microchannel. Further study into the nanolayer model looks into the surface chemistry of the nanoparticles but that will not be considered in this project as the above nanolayer equations result in an accurate enough approximation as of this time.

2.4 Nanofluid Viscosity - Background

Suspension of nanoparticles in a base fluid causes a pressure drop and consequently increases the amount of energy necessary for pumping the fluid mixture, this then proportionally influences the mixtures viscosity [11]. Experimental research done for nanofluids typically envolves a viscosity analysis over a range of nanofluid types and concentra-

tions [12–15]. There is also many proposed theoretical approaches to determining viscosity, for example Einstein [16], Saito [17], and Lundgren [18]. The theortical research done on the viscosity are based off the volume faction of the nanoparticle to base fluid. Many authors have contrasting research that include the factor of particle size and shape and temperature on the viscosity. Alternatively there are empirical correlations that have been developed, Prasher [12], but have their own shortcomings in accuracy. Prasher have propsed a model to predict the viscosity of Al_2O_3-propylene glycol setup as follows:

$$\frac{\mu_{nf}}{\mu_{bf}} = 1 + 10\varphi \tag{2.11}$$

where μ_{nf}, μ_{bf} and φ are the viscosity of the nanofluid, viscosity of the base fluid and the volume fraction, respectfully [12]. The AARD% for this correlation if 15.77%. Nguyen has prosed the following relation for the Al_2O_3-water:

$$\frac{\mu_{nf}}{\mu_{bf}} = 0.904\varphi^{0.148} \tag{2.12}$$

For 47 nm particle size, and;

$$\frac{\mu_{nf}}{\mu_{bf}} = 1 + 0.025\varphi + 0.015\varphi^2 \tag{2.13}$$

For 36 nm particle size. However, none of the above equations for approximating the nanofluid viscosity take into considerations of temperature and particle size; this leads to high errors. The following proposed equations are 1^{st} and 2^{nd} degree polynomials used in approximating the viscosity of the nanofluid Al_2O_3-water in relation to temperature.

$$\frac{\mu_{nf}}{\mu_{bf}} = 1.125 - 0.0007T \tag{2.14}$$

$$\frac{\mu_{nf}}{\mu_{bf}} = 2.1275 - 0.0215T + 0.0002T^2 \tag{2.15}$$

The above equations are valid for volume concentrations of 1% and 4%. respectfully. The equations offer much more accurate standard deviation errors of only 3.75% and 11.39%, respectfully. The downside of these equations is they are individually constructed for specific volume percentages which limit their applicability. Literature that combines theoretical and experimental research that fully consider parameters for volume concentration, temperature and particle size are required for more accurate approximations for viscosity of nanofluids can be made.

2.5 Group Method of Data Handeling - GMDH Method

The method of approximating the viscosity of the nanofluids used in the simulation process of this report is the group method of data handeling system (GMDH) that has been studied at Amirkabir University of Technology in Tehran, Iran. The viscosity of nanofluids

investigated in the GMDH method report are determined as a function of temperature, volume concentration and particle size through using a neural network system. This study by S. Atashrouz, G. Pazuki and Y. Alimoradi for determining viscosity is an advanced hybrid self-organizing polynomial neural network that has inputs of experimental data collected from hundreds of other nanofluid studies [2]. The results of this report show that the hybrid GMDH model can accurately predict the viscosity of nanofluids with a percentage of average absolute relative deviation for all systems to 2.14% with a regression coefficient of R = 0.9978. Compared to theoretical models the GMDH method exhibits a higher accuracy within the range of variables [2].

Many reports done in the field of nanofluids have theroretical models for determining various properties of a nanofluid which are then validated by experiments. The GMDH method then takes those experimental results to then construct a database of experimental data to then predict models for viscosities of the experimentally tested nanofluids. The GMDH-PNNs developed by this method that are used in this report relate to the Al_2O_3-water, CuO-water, and TiO_2-water nanofluids.

2.5.1 GMDH - General Multinomial Expression

The data handling algorithm, orginally introduced by Ivakhnenko, follows the philosophy of Darwin's theory of natural selection. The algorithm is based on the slection of the most appropriate polynomial expression built by combination of two independent variables at a time. As the algorithm iterates a general multinomial expression is gradually devised at each step. From this a grand correlation multinomial that models the entire system takes the form of Volterra-Kolmogorov-Gabor (VKG) [19]:

$$y_i = a + \sum_{i=1}^{N_v} b_i x_i + \sum_{i=1}^{N_v} c_{ij} x_i x_j + \dots + \sum_{i=1}^{N_v} \sum_{j=1}^{N_v} \cdots \sum_{k=1}^{N_v} d_{ij\dots k} x_i x_j \dots x_k \tag{2.16}$$

where, N_v stands for the number of independent variables. An N-numbered observed data set can be structured in the form of a matrix as depicted in Figure 2.3. The left matrix holds the vector of observed values $\overrightarrow{V_y} = (y_1, y_2, ..., y_n)$, while the right one represents the vector of independent variables $\overrightarrow{V_x} = (x_1, x_2, ..., x_n)$.A quadratic polynomial in terms of combination of two independent variables at a time can be proposed to estimate the actual data. Therefore, out of N_v variables, $\begin{Bmatrix} N \\ 2 \end{Bmatrix}$ quadratic polynomial can be expressed:

$$z_i^{GMDH} = aA_i + bB_i + cA_i b_i + dA_i^2 + eB_i^2 + f \tag{2.17}$$

Now, the matrix of independent variables can be defined in terms of the vector of new variables $\overrightarrow{V_z} = (z_1, z_2, ..., z_n)$ [2].

The coefficients of the above equation are then adjusted using the least square method to minimize the square deviation from the actual data for each column. The training data set is used to determine the exact coefficients after adjustment to create the most appropriate combination of variables (z_i). Deviation of the predicted results from the experimental data set must meet the pre-defined residual. The iterative process concludes once the ε is met and all previous z columns that failed to meet the criteria are omitted. the methodology for this adjustment process are as follows:

$$\delta_j^2 = \sum_{i=N_t+1}^{N} \left[y_i - z_i^{GMDH}\right]^2 < \varepsilon \qquad j = 1, 2, \ldots, \left\{ \begin{matrix} N \\ 2 \end{matrix} \right\} \tag{2.18}$$

where ε is arbitrarily chosen and N_t refers to the number of data used for training the system [2]. The total deviation of each iteration is saved and compared to that of the former calculations until the minimum value is reached. A schematic of GMDH networks is shown in Figure 2.4.

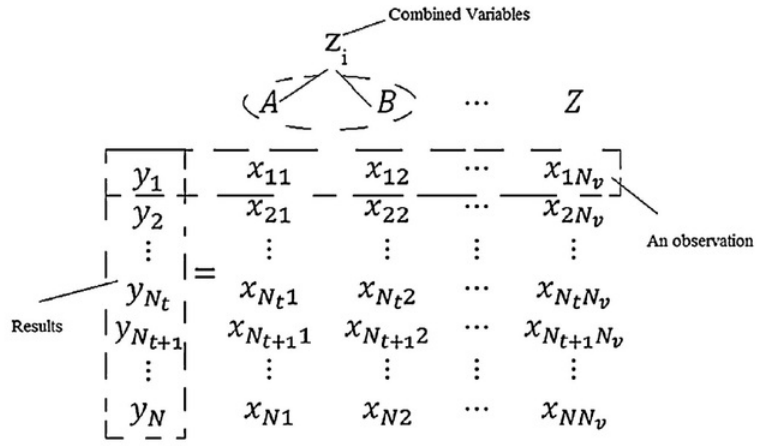

Figure 2.3: Observed data structured by a $N \times N_v$ matrix [2]

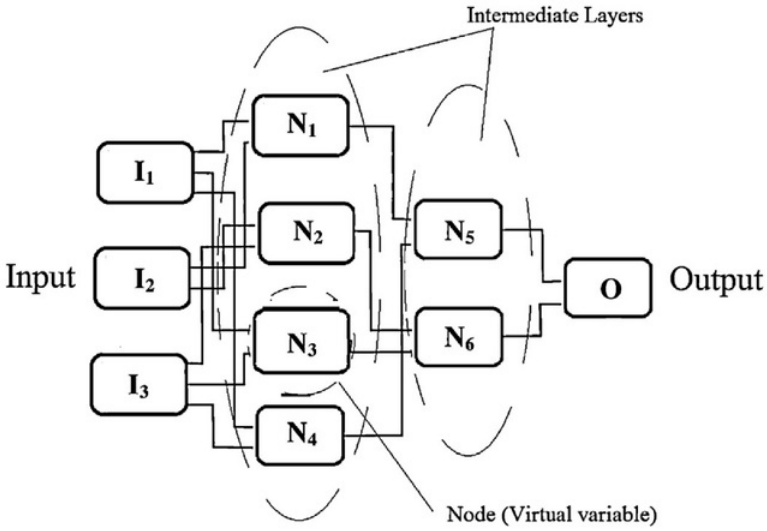

Figure 2.4: Schematic of GMDH networks [2]

System	Related GMDH-polynomial	Range of Variables	Number of data points
CuO-water	$\mu_r = 0.792034 + 36.3781\varphi -$ $408.646\varphi^2$-$0.27359N_2$ + $0.236136N_2^2$ $N_2 = 49.9132$ - $0.313024T$ - $0.22456T\varphi + 0.000502158T^2$ + $49.9962\varphi + 833.886\varphi^2$	$294 < T < 337$ $0.01 < \varphi < 0.07$ $d = 29$	54
TiO_2-water	$\mu_r = -0.439835 + 0.00491987T +$ $0.206399T\varphi - 55.5471\varphi$	$288 < T < 308$ $0.002 < \varphi < 0.02$ $d = 27$	15
Al_2O_3-water	$\mu_r = 23.1077 - 0.14405T +$ $0.00148085TN_2 + 0.000223842T^2 +$ $0.543175N_2$ $N_2 = -0.00268592 - 0.0438904dN_4 +$ $0.0438062dN_3 + 1.88848N_4 -$ $0.881516N_3$ $N_3 = 1.79002 + 14.0621\varphi -$ $0.00360243dN_4 - 0.927421N_4 +$ $0.333461N_4^2$ $N_4 = 34.9901 - 0.213666T -$ $0.0874713T\varphi + 0.000339022T^2 +$ $602.534\varphi^2$	$294 < T < 343$ $0.01 < \varphi < 0.094$ $d = 36, 47$	138

Table 2.1: Nodal expressions for hybrid GMDH-PNN [2]

2.6 Theoretical Velocity through Microchannel

Since the microchannel must maintain a lamniar flow it is important to determine a suitable pressure that sustains a low enough average velocity to maintain a Reynolds number within the laminar regime. The microchannel also has the characteristic of having no fixed vertical wall boundaries so the problem can be broken down into a system of pressure driven flow between two fixed plates. [20] The dimensions of the plates is the length and width of the microchannel at 4000 μm and 1000 μm, respectfully, which is much greater than the distance between plates, or the vertical height of the microchannel of 200 μm. Considering that $L_{x,z} \gg d.$ and a pressure drop of Δp between the the mircochannel inlet at x=0 and outlet of x=L_x, the pressure gradient becomes $G = \Delta p / L_x$.
Applying a no-slip boundary condition, $v_x(0) = v_x(d) = 0$, to the plates we obtain $A = Gd/2\eta$ and $B = 0$, so the velocity field becomes [20]:

$$v_x(y) = \frac{G}{2\eta} y(d - y) \tag{2.19}$$

This function of velocity holds a parabolic shape that decribes a laminar flow with the maximum velocity at $Gd^2/8\eta$ located at the middle distance between the plates when $y = d/2$.

From the velocity field we can integrate over the cross-sectional area of $d \times L_z$ to obtain a function of volumetric discharge rate:

$$Q = \int_0^d v_x(y) L_z dy = \frac{G L_z d^3}{12\eta} \tag{2.20}$$

The average velocity of through the microchannel can then be determined by the discharge rate by now dividing by the cross-sectional area of the microchannel, $d \times L_z$:

$$U = \frac{1}{d} \int_0^d v_x(y) dy = \frac{Q}{L_z d} = \frac{G d^2}{12\eta} \tag{2.21}$$

From this equation an average velocity can be predicted off the pressure difference, Δp, to then be put into the Reynolds Number equation to determine if the assumed laminar flow can be maintained.

2.7 Reynolds Number

In order to determine if the inlet pressure is satifactory for the microchannel simulation it must demonstrate that it produces a flow through the microchannel that falls within the laminar regime with a Reynolds Number ≤ 2300. To calculate the Reynolds Number using the average velocity through the microchannel the below equation is used [20]:

$$Re = \frac{Ud}{\nu} = \frac{Ud}{\mu/\rho} \tag{2.22}$$

where, U, d, ν, μ, and ρ is the average flow velocity, height of microchannel, and kinematic viscosity of the fluid, viscosity of the fluid, and the density of the fluid, respectfully.

Using a pressure difference of 750 Pa across the microchannel and fluid viscosity to be $9.1 \times 10^{-4} kgm^{-1}s^{-1}$ to represent liquid water, we then applying those characteristics to the dimensions of the microchannel and obtain an average fluid velociy of 0.6868 m/s. With this average velocity of 0.6868 m/s, effective diameter of $200\mu m$, visosity of $9.1 \times 10^{-4} kgm^{-1}s^{-1}$ and density of $1000 kg/m^3$ the above equations dictate that $Re = 150.9 \ll 2300$.

Chapter 3

Mathematical Models

3.1 Governing Equations for Numerical Method

The governing equations and the numerical metholodogy used for the simulation of the boundary flows are presented in this section.

Continuity:

$$\frac{\partial \rho}{\partial t} + \nabla \cdot (\rho \overrightarrow{v}) = 0 \tag{3.1}$$

Momentum:

$$\frac{\partial}{\partial t}(\rho \overrightarrow{v}) + \nabla \cdot (\rho \overrightarrow{v}\,\overrightarrow{v}) = -\nabla p + \nabla \cdot (\bar{\bar{\tau}}) + \rho \overrightarrow{g} + \overrightarrow{F} \tag{3.2}$$

$$\bar{\bar{\tau}} = \mu \left[(\nabla \overrightarrow{v} + \nabla \overrightarrow{v}^T) - \frac{2}{3} \nabla \cdot \overrightarrow{v} I \right] \tag{3.3}$$

Energy:

$$\frac{\partial}{\partial t}(\rho E) + \nabla \cdot (\overrightarrow{v}(\rho E + p)) = \nabla \cdot \left(k_{eff} \nabla T - \sum_j h_j \overrightarrow{J_j} + (\bar{\bar{\tau}}_{eff} \cdot \overrightarrow{v}) \right) \tag{3.4}$$

$$E = h - \frac{p}{\rho} + \frac{v^2}{2} \tag{3.5}$$

$$h = \sum_j Y_j h_j + \frac{p}{\rho} \tag{3.6}$$

$$h_j = \int_{T_{ref}}^{T} c_{p,j} dT \tag{3.7}$$

Solid Temperature:

$$T_w = \frac{(q - q_{rad})\Delta n}{k_s} + T_s \tag{3.8}$$

$$T_w = \frac{(q - q_{rad})}{h_f} + T_f \tag{3.9}$$

where, ρ, p ,$\bar{\bar{\tau}}$, $\rho\vec{g}$, $\vec{F}$, μ, I, k_{eff}, $\vec{J_j}$, h, Y_j, T_{ref}, T_w, q_{rad}, Δn, k_s, T_s, h_f, and T_f are density, pressure, stress tensor, gravitational body force, external body forces, molecular viscosity, unit tensor, effective thermal conductivity ($k + k_t$ where k_t is the turbulent thermal conductivity defined according to turbulence model), diffusions flux of species j, sensible enthalpy, mass fraction of species j, reference temperature of 298.15 K, wall temperature, radiative heat flux, distance between wall surface and the solid cell center, thermal conductivity of the solid, local solid temperature, local fluid heat transfer coefficient, and local fluid temperature, respectfully.

The ∇, or nabla operation used in the governing equations represents the partial derivative of a quantity with respect to all directions in the chosen coordinate system. Nabla is defined in Cartesian coordinates to be:

$$\frac{\partial}{\partial x}\vec{i} + \frac{\partial}{\partial y}\vec{j} + \frac{\partial}{\partial z}\vec{k} \tag{3.10}$$

The ∇ operator appears in several forms in the governing equations as $\nabla \cdot (\bar{\bar{\tau}})$, ∇p, and $\nabla(\vec{v})$ that result in the following operations:

$$\nabla \cdot (\bar{\bar{\tau}}) = \frac{\partial \bar{\bar{\tau}}_x}{\partial x} + \frac{\partial \bar{\bar{\tau}}_y}{\partial y} + \frac{\partial \bar{\bar{\tau}}_z}{\partial z} \tag{3.11}$$

$$\nabla p = \frac{\partial p}{\partial x}\vec{i} + \frac{\partial p}{\partial y}\vec{j} + \frac{\partial p}{\partial z}\vec{k} \tag{3.12}$$

$$\nabla(\vec{v}) = \left(\frac{\partial}{\partial x}\vec{i} + \frac{\partial}{\partial y}\vec{j} + \frac{\partial}{\partial z}\vec{k}\right)\left(v_x\vec{i} + v_y\vec{j} + v_z\vec{k}\right) \tag{3.13}$$

$$\begin{pmatrix} \frac{\partial v_x}{\partial x} & \frac{\partial v_x}{\partial y} & \frac{\partial v_x}{\partial z} \\ \frac{\partial v_y}{\partial x} & \frac{\partial v_y}{\partial y} & \frac{\partial v_y}{\partial z} \\ \frac{\partial v_z}{\partial x} & \frac{\partial v_z}{\partial y} & \frac{\partial v_z}{\partial z} \end{pmatrix}$$

When the flow enters through the pressure inlet boundary, fluent uses the boundary condition pressure input as the total pressure of the fluid at the inlet plane p_0. For incompressable flow the inlet total pressure and the static pressure p_s are related by Bernoulli's equation:

$$p_0 = p_s + \frac{1}{2}\rho v^2 \tag{3.14}$$

With the resulting velocity magnitude and flow direction vector specified as normal to boundary the velocity vector, $\overrightarrow{v}$, is computed. This then feeds into the governing equations of continuity, momentum, and energy.

3.2 Thermo-physcial Equations

This chapter contains the governing equations that are used to calculate the density, heat capacity, thermal conductivity and the viscosity of the nanofluid that are then used to numerically simulate Al_2O_3-water, CuO-water and TiO_2-water nanofluids. Since the fluid being simulated is a mixture of nanoparticles and a base fluid of water, the effective properties of the fluid must be considered. In general, these equations relate the volume percentage of the nanoparticles and the individual characeristic properties of the separate components. For the density and heat capacity of the nanofluid a simple volume percentage to properties relation is used, seen below [7]:

$$\rho_{eff} = (1-\varphi)\rho_f + \varphi\rho_p \tag{3.15}$$

$$C_{p,eff} = \frac{(1-\varphi)(\rho C_{p,f})_f + \varphi(\rho C_p)_p}{\rho_{eff}} \tag{3.16}$$

The thermal conductivity of the nanofluid however, is much more complicated and has been involved in many research papers in recent years to best depict the mechanism of thermal transfer of the fluid. To determine the thermal conductivity of the nanofluid in this project, an equation developed by W. Yu and S.U.S. Choi is used that includes the effects of nanolayers on the thermal conductivity [1].

$$k_{eff} = \frac{k_{pe} + 2k_m + 2(k_{pe} - k_m)(1+\beta)^3\phi_v'}{k_{pe} + 2k_m - (k_{pe} - k_m)(1+\beta)^3\phi_v'}k_m \tag{3.17}$$

The process for deriving this above equation is gone through indepth in Chapter 2 section 2.3. The process for arriving at this manipulation of Maxwell's equation is based on experimental studies related to nanolayers that are formed around nanoparticles during suspension in a base fluid.

The viscosity of the nanofluids are decribed by the GMDH-PNNs at the temperature of 300 K [2] seen in Table 2.1. Since the method for simulating the flow in the microchannel is based on a fixed laminar flow the method for using variable viscosity based off temperature caused extreme velocity values in the microchannel due to Fluent forcing a fixed parabolic velocity profile. Since the microchannel is on such a small scale it is important to maintain this laminar flow because of the sensitiviy to corrosion and vibration. If the variable viscosity was properly implemented into a laminar flow it would increase the accuracy of the simulation. The equations for calculating the viscosity of Al_2O_3-water and CuO-water nanofluids are shown in Table 2.1.

However, since the multinomial expression are trained on experimental data sets, the range of temperatures and volume concentrations are limited to the data sets used. For the

Al_2O_3-water and CuO-water nanofluids this doesn't interfer with this report parameters due to the ranges extending from 1% to beyond 5% but for the TiO_2-water nanofluid further methods must be used for volume concentrations of >2%. To supplement the viscosity values for the TiO_2-water nanofluid, theoretical values taken from another report done by Ann Lee, School of Engineering Macquarie, are used for simulation fluid properties [21].

3.3 Thermo-physical Properties

Volume Concentration	Nanofluid	ρ_{eff} $[kgm^{-3}]$	$C_{p,eff}$ $[Jkg^{-1}K^{-1}]$	k_{eff} $[Wm^{-1}K^{-1}]$	μ_{eff} $[kgm^{-1}s^{-1}]$
$\varphi = 1\%$	Al_2O_3-water	1029.5	4058.7	0.64936	0.001015
	CuO-water	1053.1	3937.2	0.65146	0.000962
	TiO_2-water	1032.3	4042.7	0.64311	0.001060
$\varphi = 3\%$	Al_2O_3-water	1088.5	3825.6	0.75666	0.001230
	CuO-water	1159.3	3508.9	0.75559	0.001405
	TiO_2-water	1096.9	3782.3	0.73583	0.001394
$\varphi = 5\%$	Al_2O_3-water	1147.5	3616.6	0.87719	0.001442
	CuO-water	1265.5	3152.5	0.87517	0.002023
	TiO_2-water	1161.5	3550.8	0.83837	0.004485

Table 3.1: Thermo-physical properties of the metallic nanofluids

3.4 Numerical Scheme

The governing equations for continuity, momentum, energy and solid temperature are discretised by the finite volume technique (FVM) on the meshing elements by ANSYS Fluent. The SIMPLE algorithm is used and considers the relationship between velocity and pressure to enforce mass conservation and to obtain local pressures.

The gradients are computed in Fluent according to the least squares cell-based method where the solution is assumed to vary linearly. In Figure 3.1, the change in cell values between cell $c0$ and ci along the vector δr_i from the centroid of cell $c0$ to cell ci, can be expressed as:

$$(\nabla\phi)_{c0} \cdot \Delta r_i = (\phi_{ci} - \phi_{c0}) \tag{3.18}$$

To solve for $(\nabla\phi)_0$ the calculation method is to use a least squared solution on the non-square coefficient matrix. The linear system of equations can be solved by deconstructing the coefficient matrix using the Gram-Schmidt process [22]. This process results in a gradient value with vectors in all Cartesian directions, $(W^x_{i0}, W^y_{i0}, W^z_{i0})$ are produced for each face of cell $c0$.

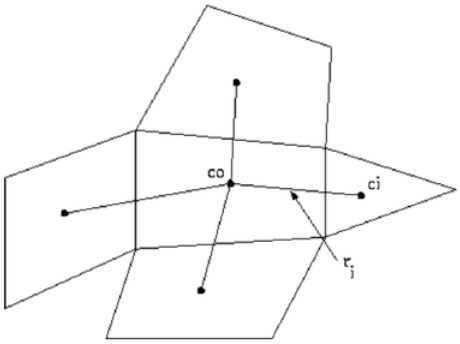

Figure 3.1: Cell Centroid Evaluation

The spatial discretization method for the pressure is second order for the improved accuracy. The momentum and energy discretization method used is the second-order upwind scheme, this increases accuracy as it considers the cell faces as a multi-dimensional linear reconstruction. This approach is achieved at cell faces through a Taylor series expansion of the cell-centered solutions about the cell-centroid. Thus, when second-order upwinding is selected, the face value ϕ_f is computed using the following ezpression:

$$\phi_{f,SOU} = \phi + \nabla\phi \cdot \overrightarrow{r} \tag{3.19}$$

where ϕ and $\nabla\phi$ are the cell-centered value and its gradient in the upstream cell, and $\overrightarrow{r}$ is the displacement vector from the upstream cell centriod. However, this formulation requires that the gradient $\nabla\phi$ of each call is already determined. The iterative process in determining the numerical values of each cell are continuous until x-velocity of the fluid has reached its residual of 10^{-6}, at such a point the calculation concludes. Verification of this residual is based on the change in thermal performance results between $(10^{-6} - 10^{-7})$ and is justified in Chapter 5. The velocity of the fluid entering the inlet faces is determined using Bernoulli's equations at a direction vector that is normal to the faces. The outlet faces have a realitive pressure of 0 Pa with reverse-flow determined by adjacent cells with direction vectors normal to the outlet face. Symmetry boundaries on the front and back faces of the MCHS have no-slip wall conditions with heat flux and velocity set to 0.

Chapter 4

Simulation Model

The nanofluids investigated for their thermal performance are Al_2O_3-water, CuO-water, and TiO_2-water at variable volume percentages of 1-5% to determine the most effective heat transfer fluid. To do this, a geometry must be designed to test numerical methodology to compare the individual nanofluids ability to remove heat from a system. The choice of geometry model is comprised of a microchannel that forces the nanofluid to flow across a heated silicon surface from an open inlet zone through to an open outlet zone. Below is a wireframe diagram of the geometry that represents the MCHS:

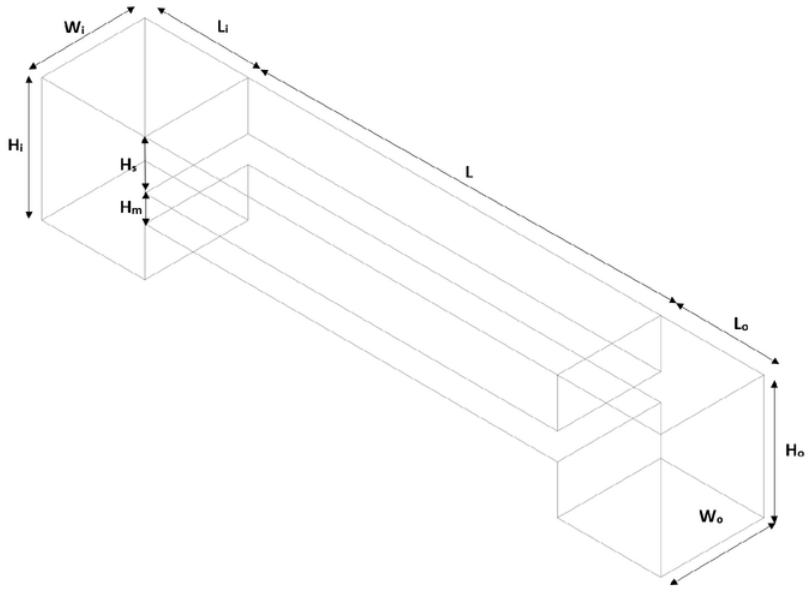

Figure 4.1: Wireframe model of simulation geometry for the MCHS showing dimensions

The fluid enters the inlet zone on the left with a height of $H_i = 1200\ \mu m$, width of $W_i = 1000\ \mu m$, and depth of $L_i = 1000\ \mu m$. Once the nanofluid has entered the inlet it is directed into the microchannel that has a height of H_m =200 μm, and placed at the bottom surface of the silicon chip $H_s = 500\ \mu m$ from the top surface of the inlet. The top surface of the silicon chip is the heating source of this model with a heat flux of $1\frac{MW}{m^2}$. Both the micrcochannel and silicon chip extend L = 4000 μm and connect to the fluid outlet of height of $H_o = 1200\ \mu m$, width of $W_o = 1000\ \mu m$, and depth of $L_o = 1000\ \mu m$. The total length of the model is 6000 μm. Since the simulation is being done as a 2D model the width of the zones isn't important in calculations of the results.

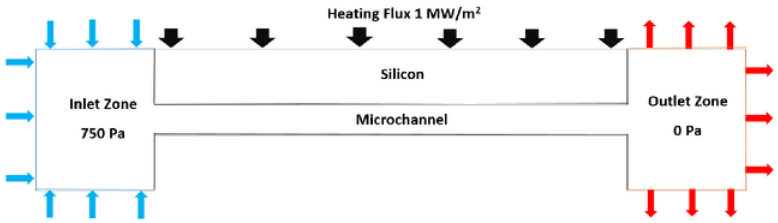

Figure 4.2: Wireframe side view of simulation model showing zones and heat flux surface

4.1 Meshing Approach

The simulation model is treated as a 2D face that is a single element thick with a total number of elements of 384,600. The meshing for the MCHS model focuses on the boundary layers in the microchannel primarily to ensure accurate heat transfer value at the liquid-solid interface is calculated. To do this edging bias has been put into place to create ultra-fine mesh elements throughout the microchannel and other liquid-solid interfaces. Another edge sizing area includes the internal boundaries of the solid silicon zone that is sized to create fine mesh at the solid-liquid interfaces but it not refined to as high of a degrees as the fluid domain. The input and output zones also are finely meshed to ensure that the numerical methodology used in the Fluent calculations is able to accurately converge both the input and output flows. It was found that irregular output flows occur with substantial backflow on outlet faces because of the low pressure zones formed on either side of the microchannel outlet but was resolved once more fine mesh elements were generated.

Element meshing has been focused on the liquid zone from the inlet through the microchannel into the outlet because the fluid momentum and energy calculations are be the main convergance condition for this numerical method. However, since the version of the program being used for these models and simulation is ANSYS Workbench 18.1 Academic version there are limitations to the number of elements contained in the mesh. The final mesh for this project contains 384,600 elements which is under the limitations of the academic version of the software but accpetable when describing a 2D shape.

4.1.1 Microchannel

To create a fine boundary layer for the meshing of the microchannel a bias was used which creates a mesh that becomes finer on either end of the edging. To do this the exterior two edges of both the inlet and outlet zones were selected to create an edge sizing condition. This edge sizing is of type *Number of Divisions* set to 300 divisions. The behaviour is set to soft and the bias factor is set to 12. This allows for a reasonable growth rate between the boundary of the microchannel and the centre of the microchannel. This method give a minimum element height of approximately 4×10^{-7} m at the boundary of the microchannel and a maximum element height of approximately 2×10^{-6} m. The element width is fixed through the whole microchannel at 4×10^{-6} m, this can be improved through increasing the number of divisions along the x-axis of the microchannel from 1000 to $\geq$ 1000 divisions but is not necessary.

4.1.2 Solid Domain

The silicon zone of the model is the only solid component of the design so only the solid temperature mathematical euqations are calculated. This means that the elemenets required to depict these details doesnt need to be on the same magnitude as the fluid domain in the model. However, certain methods of dividing this zone was used to highlight the solid-liquid interface zones to ensure reliability in the heat transfer region of the model where Equation 3.9 is used. Both the vertical and horizontal edges of the silicon section were sized with bias that created fine mesh at the interface zones with bias factors of 12. Since the top surface is only a fixed heat flux zone the number of elements did not need to be as high. The silicon zone has 40 elements in the vertical y-axis and 300 divisions in the horizontal x-axis, giving a total number of elements to be 12,000.

4.1.3 Inlet Zone

The inlet zone meshing method was to highlight both the area where the inlet zone meets the input to the microchannel and the area in contact with the front surface of the silicon chip. Since the edge sizing used to create the elements at the microchannel boundary layer used the edges in the inlet zone as reference, the area in front of the microchannel input is already finely meshed. See Section 4.1.1 for more details on y-axis edge sizing of inlet zone. The x-axis bias that was implemented controlled the size of the mesh from the furthest face of the inlet zone to the closest face of the silicon chip. A *Number of Division* type bias was also used in this zone to control the size of mesh when approaching the silicon chip and the microchannel input. 150 divisions for the inlet zone in the x-direction was used with a bias factor of 12.

4.1.4 Outlet Zone

The outlet zone was meshed similarly to the inlet mesh because they have identical geometries. However, to allow for successful convergence of the flow exiting the microchannel,

more divisions were used to allow for smaller element size to allow for quicker convergence. The number of divisions in the x-axis is 300 compared to the 150 divisions for the inlet zone. Once, this increase in divisions was applied, the turbulence of the flow was settled in approximately 2000 less iterations of the calculations.

4.2 Simulation Set-Up

The numerical calculation applied to this geometry have been simulated as steady fluid flow to best highlight the overall thermal performance of the nanofluids in a steady-state. To ensure realistic results the pressure difference between inlet and outlet zones is fixed at 750 Pa to both keep the fluid flow in the laminar regime with a low Reynolds number and to allow the viscosity to impact the results which would not occur during a fixed velocity inlet. If this project was experimental based the testing would have to be pressure based flow because it would be impossible to calibrate velocity and mass flow rate for each of the nanofluids reliably.

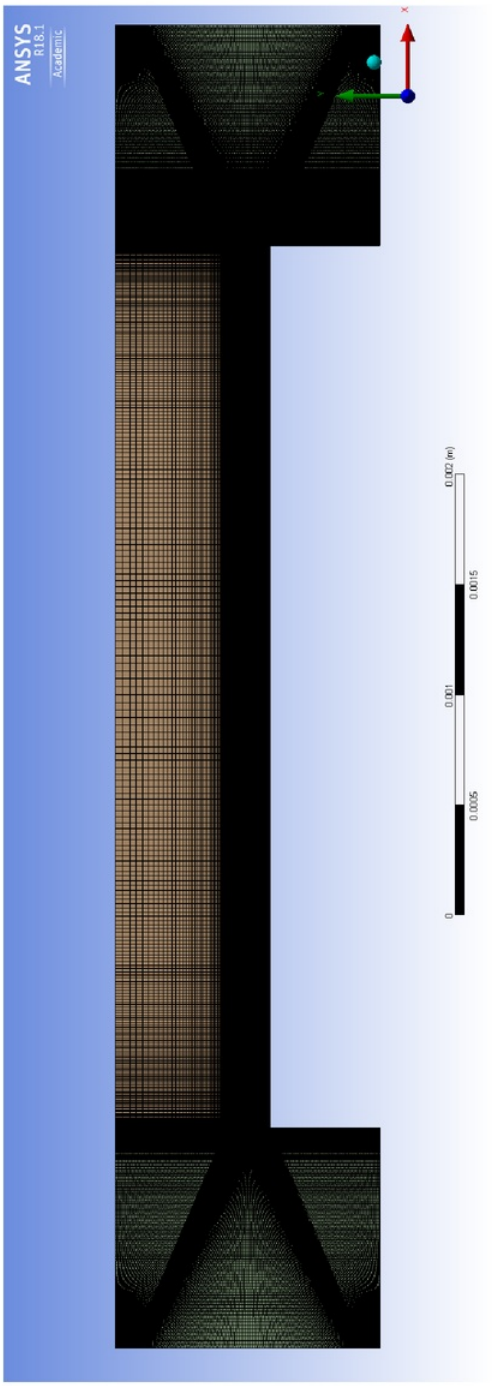

Figure 4.3: Full side view of the meshing elements used in the MCHS geometry model

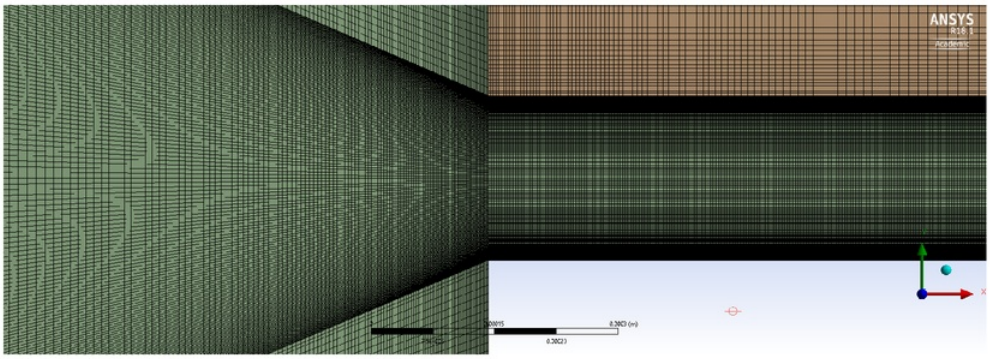

Figure 4.4: Close view of the input to the microchannel from the inlet zone

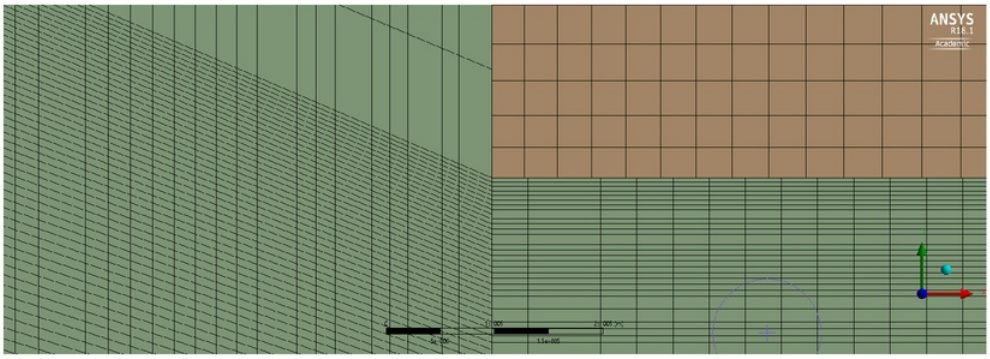

Figure 4.5: Detailed view of the junction between meshing domains

Chapter 5

Verification

The word verify (from the Latin, *verus*, meaning true) means to assert or establish truth. To confirm that a model is verified is to say that the model demonstrates truth or shows that there is a reliabily in the methodology. However, it is impossible to demonstrate the truth of an proposition except in a closed system. For a given proposition it follows symbolic logic that if "p" entails "q", we know that if "p" is true, then "q" is true if and only if the system that this formalism represents is closed. An example for an open system where this logic fails is if the statement is said, "If it rains tomorrow I will stay at home". Then the next day it rains, but the person leaves home, the verification will fail in that case. The statement is true because the intention was true but did not guarantee the outcome because it did not consider outside variables that could influence the decision to stay or leave. Purely formal structures such as mathematical models are verifiable because they can be proved by symbolic manipulations, and the meaning of these symbols is fixed and not contengent on empirically based input parameters [23].

Numerical models may contain closed mathematical compononets that may be verifiable, just as an algorithm within a computer program may be verifiable. Mathematical components are subject to verification because they are part of closed systems that include claims that are always true as a function of the meanings assigned to the specific symbols used to express them. Numerical methods that are determined by clearly defined mathematical equations are confined to the limitations to those functions to ensure the verification of the system. For complex open system it is logical to assume that there are close systems buried within the open system, such as the governing equations of physics apply to open systems although they may not determine the outcome of all scenarios. However, the models that use mathematical models are never really exclusively closed systems either. For example, the Mechanical Engineering related mathematical models for momentum, thermal conductivity, viscosity , etc. are all base on incomplete data sets that are only approximately known. There will always be a loss of information for any system because not all aspects of a system can be modeled because the loss is inherent in the continuum mechanics approach [23].

The mathematical models used by default in ANSYS Fluent are based on theoretical principles that has be experimentally verified to accurately approximate realistic actions.

For example, the equations of velocity through the microchannel is based off Bernoulli's principles for incompressible flow and are considered accurate for those characteristic flows. But the assumption made for the incompressiblity of the fluid can be improved to the compressible flow equations even if the alteration provides negligible change in results the model would still be considered more accurate. For the verification of the numerical method for simulating the thermal performance of the HTF of various nanofluids in the MCHS the residuals for the calculations are tested to provide the condition where the mathematical models are calculating to the highest accuracy while reducing the amount of time required per simulation calculation.

Verification of the closed simulation model system compares the temperature distribution profiles across the bottom surface of the silicon chip at the converging residuals of 10^{-4} to 10^{-7}. Results from the base pure water, with no nanoparticle suspension, numerical simulation is used to verify the numerical methodology of the governing equations. The following simuation tests for the metallic nanofluids follow from replicated set-up models of the chosen liquid water with desired residuals. The largest residual with the least difference from the next order of residuals is be chosen to save time in the simulation process.

The results of this residual comparison is to use 10^{-6} as the convergance residual for the x-axis velocity of the microchannel simulation. The x-axis residuals have the slowest rate of convergance when below 10^{-4} residuals so only the x-axis residual is be set to 10^{-6}.

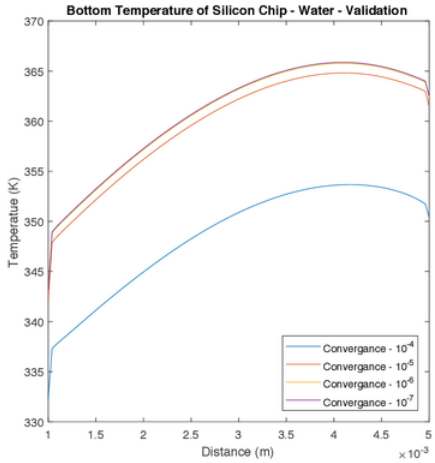

Figure 5.1: Validation of the simulation method by comparing the bottom temperature of the silicon surface against the convergance value

Chapter 6

Impact of Density and Heat Capacity on Thermal Performance

6.1 Influence of Density on Thermal Performance

The density of a material is described by the amount of mass per unit volume of space and has the S.I. units of kg/m^3. The density of a fluid used in the application of a HTF for a MCHS is important as it relates strongly to other thermo-physical properties that can determine the overall thermal performance of the fluid. For nanofluids, the partical concentration of the nanoparticles directly determine the density of the nanofluid by using the relationship shown in Equation 3.15. Applying this method for determining density on the nanofluids yield a range of density ranging from 1029.5-1265.5 kg/m^3, seen in the Table 3.1.

The individual influence of density on the thermal performance of a HTF as a stand alone property is that for increased density comes increased mass. Adding more mass to a system without changing the thermal conductivity, viscosity, or dimensions of the model will cause the heat capacity to work more effectively. With the enhanced heat capacity the thermal load of the system increases and can affect the efficiency of overloaded systems. The difference in density of the nanofluids compared to the base water however, only vary from between 2.9-26.6% so the impact of density is limited when other thermo-physical properties such as viscosity range from 5.7-493.0% realitve to base water properties. In the application of nanofluids it is clear that the thermal performance is determined more by the thermal conductivity and viscosity.

6.2 Influence of Heat Capactiy on Thermal Performance

The influence of heat capacity on the thermal perfomance of the MCHS is related to the amount of energy per unit of mass the material can hold before the material increases in temperature. The affect having a higher heat capacity has on the thermal performance can

relate to the thickness of the boundary layer. When the HTF is cooling the silicon surface the fluid cells are able to absorb more thermal energy until the condition that $T_f = T_w$ where no thermal energy flow occurs, $q = 0$ based on Equation 3.9. Since increasing heat capacity independantly of other thermo-physical properties allows for a higher storage of thermal energy without the necessity of increased mass means that the fluid cells are able to hold more energy before increasing in temperature which stunts the growth of the thermal boundary layer. The mechanism for thermal boundary layer growth is outlined in Section 7.1.1. Compared to the base fluid the heat capacity of the nanofluids range from percentage decreases of between 3.0-24.7%. The nanoparticles negatively affect the ability of the water to hold thermal energy because metallic materials have the tendancy to quickly allow thermal energy to flow through them due to a high thermal conductivity and not to insulate or store the energy. However, similar to the affect density has on the thermal performance, the negative interaction the heat capacity has on the thermal performance is outweighted by the affects of the thermal conductivity and viscosity.

6.3 Relationship between Density and Heat Capacity

The four thermo-physical properties related to the thermal performance of the nanofluids numerically investigated in this report are all intrinsically linked. Density and heat capacity have the specific interaction of collectively determining the amount of thermal energy the system can hold at once. As density increases due to the addition of nanoparticles the overall mass of the nanofluid within the MCHS also increases. With the addition of more mass into the system the heat capacity dictates that more units of thermal energy can be contained before the condition where $T_f = T_w$. Maximising these properties will collectively enhance the thermal performance of the HTF. However, as described in Section 6.2, the addition of metallic nanoparticles into the base fluid of water subsequently lowers the heat capacity, effectively cancelling out the benefits gained from increased density. This is a major reason why the thermal conductivity and viscosity are the main contributing factors to the thermal performance over the density and heat capacity.

Chapter 7

Impact of Viscosity on Thermal Performance

7.1 Impact of Viscosity on Fluid Velocity

Contributing factors that determined the characteristics of fluid flow through the MCHS are the fluid viscosity and set parameters such as, pressure difference from inlet to outlet , Δp, forced laminar flow, no slip walls, and steady state calculation method. The set constraints that relate to the numberical methodology were held consistant across all the fluid simululations, this means that fluid viscosity is the only variance between fluids that influence the velocity through the MCHS. Although there is literature on the effect temperature has on the viscosity of all the metallic nanofluids tested, it was found to be difficult to resolve an accurate velocity profile in the microchannel that had a laminar flow and a variable viscosity. The constant viscosities taken at 300 K still, however, correspond accurately with the average velocity in the microchannel to show an expected relationship.

To promote flow over the silicon surface through the MCHS, a realitive pressure of 750 Pa was placed on the inlet, this induced an average velocity of $0.502m/s$ determined by Bernoulli's principles, seen in Equation 3.14, of the pure water. Since the pure water has the lowest viscosity of $9.1 \times 10^{-4} kgm^{-1}s^{-1}$ and the highest average velocity $0.502m/s$ out of all the tested fluids, this confirms that there is a proportiality between these two values. Calculations done for determining the Reynolds number of the flow in Section 2.6 show the $\frac{1}{\eta}$ ratio viscosity has on average flow velocity in Equation 2.21. The comparison projected onto the nanofluids also follows this trend seen in Table 7.1 and Figure 7.1 for Al_2O_3, Figure 7.2 for CuO and in Figure 7.3 for TiO_2.

The velocity profiles also describe laminar flow through the microchannel where the maximum velocity is in the center of the microchannel with stationary fluid on the top and bottom walls. The highest viscosity of the nanofluids is for TiO_2-water at 5% volume concentration at $4.4851 \times 10^{-3} kgm^{-1}s^{-1}$ and shows in Figure 7.3 to only have a maximum velocity of $0.2m/s$, which is less than one third the maximum velocity of the base water. The nanofluid with the lowest viscosity is CuO-water at 1% volume concentration

at 9.62×10^{-4} and is comparible to the base water viscosity with only a 5.7% increase. This correlates to an average and maximum velocity that are 7% less than base water at $0.469m/s$ seen in Table 7.1 and $0.705m/s$ seen in Figure 7.2. This confirms that the viscosity influences the velocity in the microchannel for both high and low realitive viscosities.

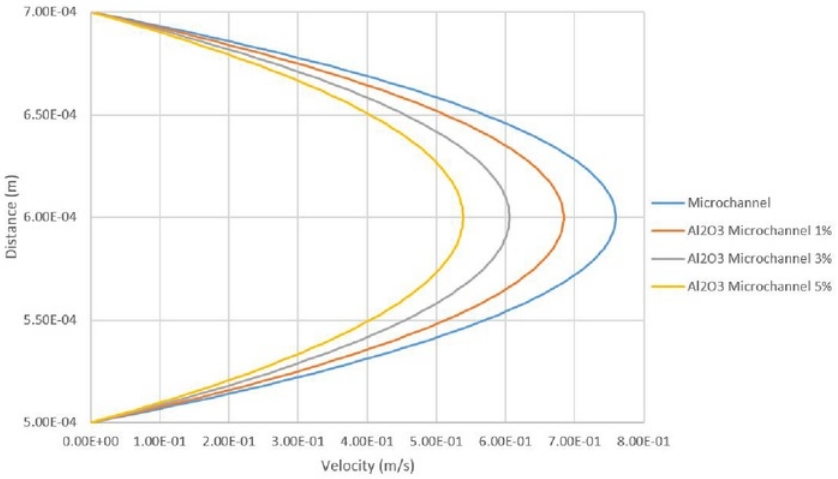

Figure 7.1: Affect of Volume Concentation on Velocity profile of Al_2O_3 nanofluid flowing through microchannel

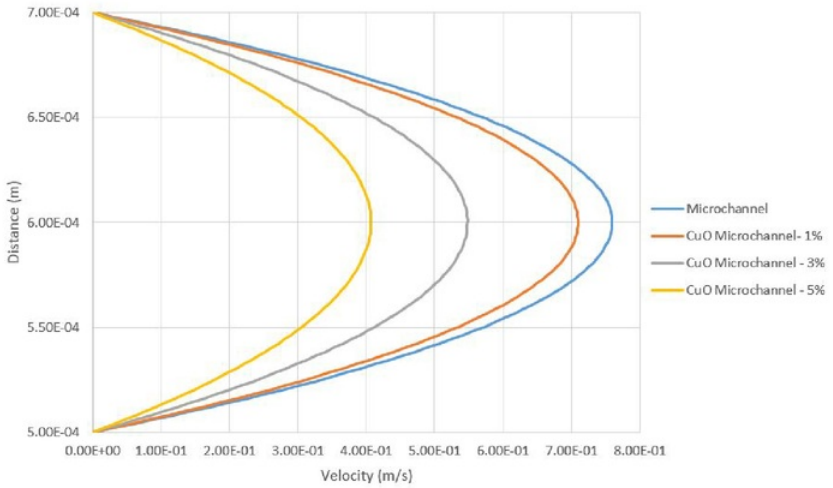

Figure 7.2: Affect of Volume Concentation on Velocity profile of CuO nanofluid flowing through microchannel

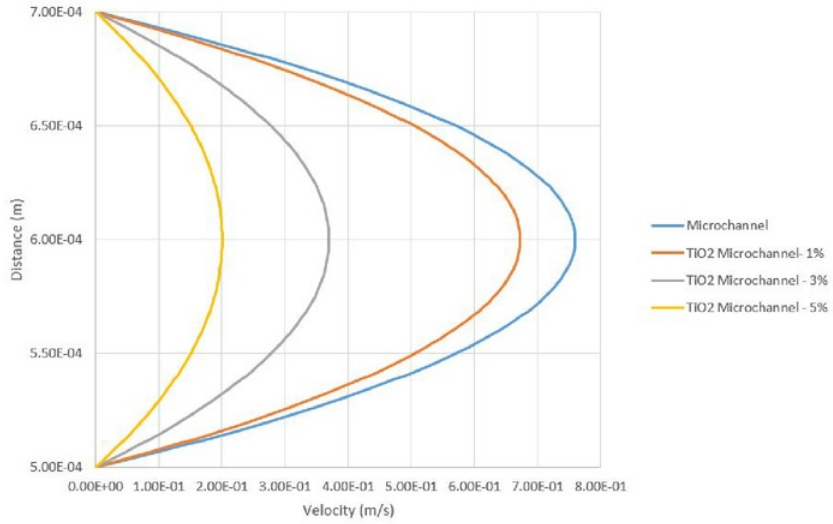

Figure 7.3: Affect of Volume Concentation on Velocity profile of TiO_2 nanofluid flowing through microchannel

Table 7.1: Average velocity in the microchannel and maximum temperature on the bottom surface of the silicon chip

	Water	Al_2O_3			CuO			TiO_2		
Volume Concentration	-	1%	3%	5%	1%	3%	5%	1%	3%	5%
Average Velocity (m/s)	0.502	0.452	0.400	0.356	0.469	0.363	0.268	0.444	0.244	0.132
Maximum Temperature (K)	365.77	365.35	361.73	358.48	364.62	364.29	364.95	366.09	373.61	384.39

7.1.1 Affect Velocity has on Thermal Boundary Layers

The thickness of the thermal boundary layer along the top surface of the microchannel is related to the viscosity of the fluid, and hence, also the velocity. As seen in Table 7.1 the increase in the average velocity of the microchannel across all numerically simulated fluids correspond to thickening of the thermal boundary layer from maximum thickness of 85 μm to the full width of the microchannel at 200 μm depicted in Figures 9.2 - 9.5.

From the moment the fluid enters the microchannel, thermal energy is transfered into the fluid at a rate q base on the temperature difference, $\Delta T = (T_w - T_f)$ seen in Equation 3.9, as the fluid continues along the microchannel it gains energy until the temperature of the fluid, T_f is equal to the temperature of the wall, T_w in which case $q = 0$. The graphs in Figure 9.1 show how for all fluids that are numerically simulated the bottom surface of the silicon increases in temperature along the microchannel to depict how the q value becomes lower as the temperature of the fluid rises. Once this event occurs the energy from the fluid close to the wall must exclusively be transfered into neighbouring fluid cells where $T_{f,0} > T_{f,1}$. This is the mechanicism that builds the thermal boundary layer until the condition where the last neighbouring fluid cell has $T_{f,n+1} = 300K$ and $q_{n+1} = 0$ or the bottom of the microchannel is met where $q_w = 0$. Increasing the velocity of the fluid through the micorchannel allows for the fluid to enter the outlet zone before the last fluid cell in the thermal boundary layer reaches a temperature of $T_{f,n} > 300K$. At volume concentrations of 5% only the TiO_2-water nanofluid formed a thermal boundary layer of width > 200 μm.

7.2 Influence Fluid Visocity has on Thermal Performance

Large thermal boundary layers reduce the value of $\Delta T = (T_w - T_f)$ at the solid-liquid boundary so the heat transfer q is also reduced, shown by the increase in temperature along the microchannel in Figure 9.1 and based on the solid temperature mathematical model of Equation 3.9. Decreasing the viscosity to reduce the thermal layer thickness directly relates to the heat transfer rate across the solid-liquid boundary at the bottom of the silicon surface and for the liquid-liquid cells within the microchannel. As mentioned in Section 7.2, the mechanism that builds the thermal boundary layer relates to how the thermal energy flows from the silicon surface through the fluid cells in the microchannel. If the thermal boundary layer has a thickness of $d_{therm} < H_m$ then the maximum amount of thermal interaction at the surface of the silicon and between the fluid cells within the microchannel has occured. In the case where the thermal boundary layer thickness $d_{therm} > H_m$ then the bottom surface of the microchannel severly reduces the efficiency of the thermal energy transfer as the surface has a fixed heat flux of 0 $\frac{W}{m^2}$. In an extreme case at length L_n, where $L_n < L$ the thermal heat transfer rate across the microchannel becomes zero. This would result in the fluid temperature across the microchannel at position L_n to be equal at all y positions, $0 < y < H_m$.

Chapter 8

Impact of Thermal Conductivity on Fluid Flow

The thermal conductivity of the nanofluids is calculated using the thermo-phsical property formula decribed in Equation 3.17. This method for calculating effective thermal conductivity is determined by the size of the nanoparticles, thermal conductivity of the nanoparticle, base fluid and nanolayer, and then then thickness of the nanolayer. The assumptions made for calculating the thermal conducitivity were that each of the nanofluids had particles of the same size of $10nm$ and equal nanolayer thickness of $2nm$. The thermal conductivity was also assumed to be ten times as conductive as the base fluid medium of water, $k_{nanolayer} = 10k_m$. Since the nanofluids are treated as a homogeneuous fluid throughout the MCHS these assumptions can be made but are unlikely able to be replicted in an experimental study without considering inaccuracies in the process.

8.1 Affect Thermal Conductivity has on Thermal Boundary Layer

Thermal conductivity dictates the ability for thermal heat energy to flow through a material and is measured in watts per square metre of surface area for a temperature gradient of one kelvin for every metre thickness. To increase the thermal conductivity it effectively increases the thermal energy transfer rate a material is physical capable of handling and is a key aspect of any HTF. The affect thermal conductivity has on thermal boundary layers is it promotes the growth of the layer off the silicon surface and into the microchannel to be removed from the system. Based off Equation 3.9, the thermal conductivity controls the rate of heat transfer q in terms of the temperature difference of the two neighbouring cells, ΔT. As q is increased the heat from the silicon surface is able to penetrate the microchannel and be physically removed from the system once contained within the fluid cell. However, since the thermal conductivity acts in terms of the temperature gradient between two neighbouring cells the maximum efficiency only occurs when the thermal boundary layer contains the largest maximum ΔT. If the thermal boundary layer is then

overly developed and has a thickness $d_{therm} > H_m$, the minimum temperature of $T_{f,n}$, at H_m and $L_n \leq L_m$, along the microchannel is expected to be $T_{f,n} > 300K$ so ΔT is reduced.

To design a maximum efficiency MCHS for a specific nanofluid or other various HTF the ideal thermal boundary thickness would be that of exactly the width of the microchannel. This design would maximise the affects of the thermal conductivity to generate the highest q rate of the system and would eliminate the zero efficiency fluid stream along the bottom surface of the microchannel that remains at constant temperature, $T_{f,inlet} = T_f$.

8.2 Influence of Thermal Conductivity on Thermal Performance

Without the thermal conductivtiy the fluid flowing through the MCHS would not be able to transfer any heat energy from the silicon surface and would not reduce the temperature of the silicon chip. The comparitive value for thermal conductivity in this report is based on water at $0.6W/mK$ and the nanofluid thermal conducitivties are calculated with expected increases of between $0 - 60\%$ based on literature of nanofluids. Independantly, the thermal conducitivty of the nanofluid would increase the thermal performance even with an overdeveloped thermal boundary layer because it is such an influential property. With the calculated thermal conductivities of the nanofluids Al_2O_3-water, CuO-water and TiO_2-water show enhancements of between $7.2-46.2\%$ all thermal performances improved based on this property. An extreme example that increasing the thermal conductivity wouldnt increase the efficiency of a system is if the MCHS was designed for a specific HTF with a thermal boundary layer that perfectly spanned the width of the microchannel. Increasing the thermal conductivity would still increase the effectiveness of the system but would technically reduce the efficiency of the system as the thermal boundary exceeds the microchannel width.

Chapter 9

Results

9.1 Discussion

The thermal performance of the nanofluids are based on the thermo-physical properties of density, heat capacity, thermal conductivity, and viscosity. To display the overall thermal performance of the nanofluids compared to the pure liquid water, temperature contours at $z = 0$ of the simulation geometry and temperature values from the bottom surface of the silicon surface have been taken to show how the $1\frac{MW}{m^2}$ entering the system affects the temperature of the silicon chip. The common features of the nanofluids are the formation of the thermal boundary layers seen in Figures 9.2 - 9.5 and the temperature of the bottom silicon surface curves seen in Figure 9.1. The thermal boundary layers begin to form on the leading edge of the microchannel as the silicon surface begins to transfer heat into the fluid from the front facing surface. Once the fluid turns into the microchannel the thermal boundary layer begins to thicken dictated by the thermo-physical properties of the fluid. The thermal heat energy removed from the silicon surface decreases as the thickness of the thermal boundary layer increases, decribed in section 7.1.1. The temperature of the bottom surface reaches it maximum value at approximately 3/4 through the microchannel as the back face connected to the outlet zone begins to cool the silicon chip as shown in Figure 9.1 for all numerically simulated fluids. When the bottom surface of the silicon is at its local maximum temperature the affects of the thermal transfer rate, q are minimised.

At 358K, industrial integrated circuits begin to become damaged through overheating so for this numerically simulated project the requirement is to reduce the maximum temperature of the pure water cooling from 365K to $\leq$358K. Out of the tested nanofluids only the Al_2O_3-water was able to approach this temperature requirement at 358.48K for a 5% volume concentration seen in Figure 9.1. However, the input temperature of the nanofluid was kept at the default of 300K which is slightly higher than usual ambient temperature and well above possible temperatures the HTF can be cooled to. Taking these factors into consideration suggests that out of the three nanofluids Al_2O_3-water is the most viable option as a HTF alternative to pure liquid water.
Although the numerical models determine that CuO-water and TiO_2-water nanofluids are undesirable alternatives there are still interesting characteristics that were highlighted

through both simulations.
For example, although the CuO-water was not able to reduce the maximum temperature compared to the pure liquid water by more than 2 K it successfully demonstrate a relationship between the thermo-physical properties. The CuO-water results show that reguardless of concentration the maximum temperature on the bottom of the silicon surface stayed consistant at 364.5±0.5K. This suggests that there is a family of thermo-physical properties that are able to produce almost exactly the same heat transfer results. It appears that the relationships between thermo-physical properties can, in a way, cancel out the positive and negative benefits of thermal performance when incorporating the CuO nanoparticles into the pure water mixture.
Contrasting the Al_2O_3-water nanofluid results of the TiO_2-water nanofluid displayed maximum temperature increase at all volume concentrations. At no concentration did the TiO_2-water nanofluid perform more effectively than the pure liquid water models, this means that the most efficient concentrations is the nanofluid with the least amount of TiO_2 nanoparticles within parameters of 1-5%. At 5% volume concentration the TiO_2-water nanofluid developed a thermal boundary layer that spanned across the full width of the microchannel which severly reduced the efficiency of the thermal performance seen in Figure 9.5. Some research suggests that at low concentrations between 0.2-2% TiO_2 nanoparticles can increase performance but not at the same level as the Al_2O_3 and CuO mixtures. The viscosity of TiO_2-water increases at a high gradient that can not be subsidized by the increased thermal conductivity.

The thermal boundary layers of each of the numerically simulated fluids begin to develope initially at the leading edge of the microchannel but as the volume concentration goes from 1-5% and the viscosity increases which allows for more time for the thickness to grow. As explored in Section 7.1 and 8.1, the viscosity and thermal conductivity are thermo-physical properties that promote thermal boundary layers and allow for growth but only the heat capacity has any real impact of reducing the thermal layer thickness. The mathematical models used for the thermo-physical properties used in this report show that density and heat capacity changes, even at the highest concentrations, do not substantially differ to that base water so their influence is shadowed by the effects of the thermal conductivity and viscosity. This is seen in Figure 9.4 where the thermal performance is relatively similar to the base fluid of water, discussed further in Section 9.1, but the thermal boundary layer is almost doubled in size to cover over 50% of the microchannel width.

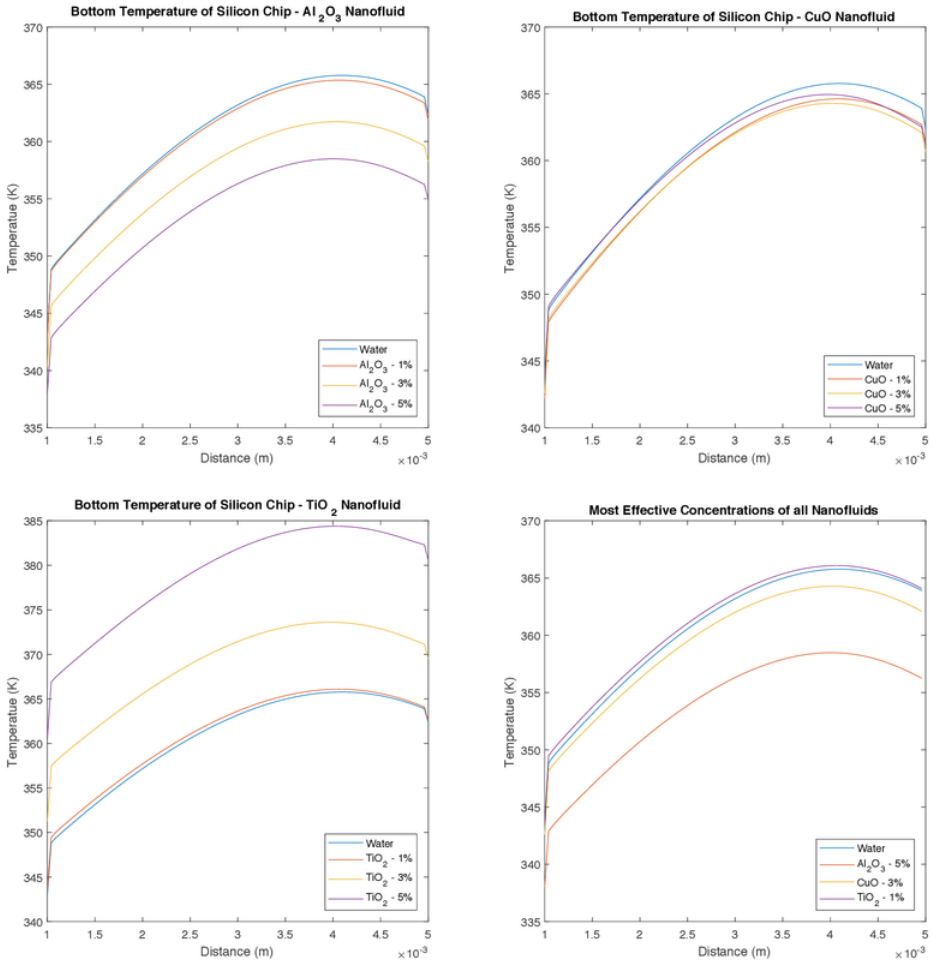

Figure 9.1: Temperature of the bottom surface of the silicon chip along the length of the microchannel comparison between the simulated nanofluids Al_2O_3-water (top left), CuO-water (top right) and TiO_2-water (bottom left)and a collection of the most effective nanofluid concentrations(bottom right)

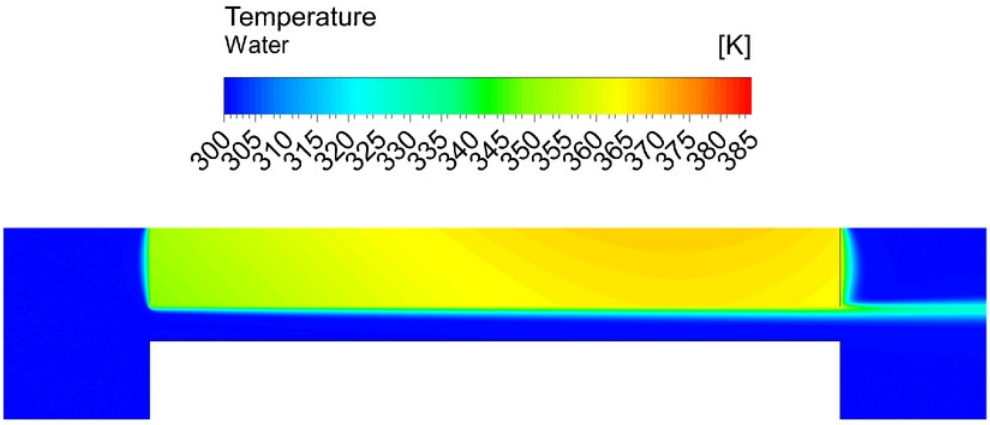

Figure 9.2: Pure Liquid Water Temperature Contour

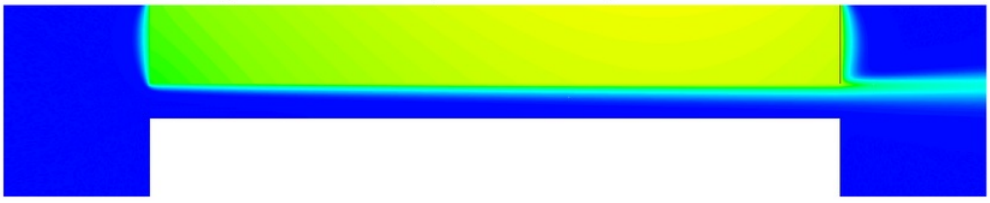

Figure 9.3: Al_2O_3-water - 5% Temperature Contour

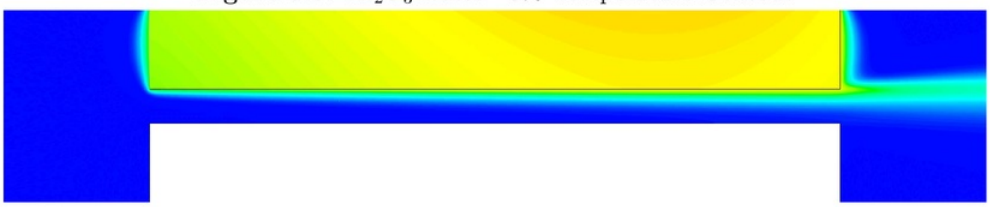

Figure 9.4: CuO-water - 5% Temperature Contour

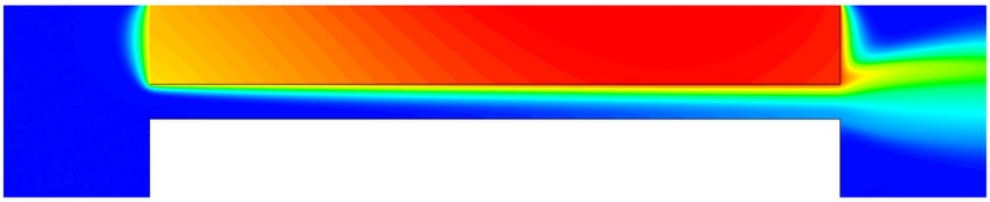

Figure 9.5: TiO_2-water - 5% Temperature Contour

9.2 Conclusion

The thermo-physical properties calculated using the mathematical models were used as inputs to ANSYS Fluent using the simulation geometry and meshing to then be calculated to a residual of 10^{-6} convergance on the x-axis velocity value. The process has been verified and the results reflect accurately the problem desribed in this report. The results of this simulation process show the ideal volume concentration of each metallic nanofluid that remove the maximum amount of thermal energy from the silicon chip. For the Al_2O_3-water, CuO-water, and TiO_2-water nanofluids the most effective concentrations are 5%, 3%, and 1%, respectfully. The thermo-physical properties of thermal conductivity and viscosity of the nanofluid demonstrated to be the largest contributing factor in the effectivenss of the HTF on the MCHS. However, out of the most effective volume concentrations of each nanofluid simulated the Al_2O_3-water at 5% showed the highest thermal performance and most closely approached the minimum temperature requirement of 358 K for the use in a computer cooling system. Al_2O_3-water at 5% volume concentration is considered the only viable alternative to water as the HTF in the MCHS system.

9.3 Future Work

Possible improvements that could be implemented in future research related to increasing the accuracy of the numerical method approach include using alternative mathematical equations to describe the model. Adjusting the governing equations to better suit the micro-scaled model and to more realistically describe the flow within the microchannel by including coefficients of roughness for the surfaces would increase the ability for the methodolgy to decribe reality. Implementation of the variable viscosity is another area that could be used in future research as the literature is available but could not be implemented in this project due to the ridgid forced laminar flow profile depicted by Fluent. A range of methods for determining thermal conductivity could be implented for comparison and relationships between approaches.

An experimental comparison for the nanofluids invesitgated in this report could also be done to validate the results of the numerical methodology. Future areas of investigation can also look at a more continuous range of volume concentrations that continue beyond 5% to show how the thermo-physical properties act at high volume concentrations.

Chapter 10

Abbreviations

HTF	Heat Transfer Fluid
MCHS	Microchannel Heat Sink
GMDH	Group Method of Data Handeling
GMDH-PNN	Group Method of Data Handeling - Polynomial Neural Network

10.1 Nomenclature

r_o	Radius of nanoparticle	(m)
k_{eff}, k_{pe}	Effective Thermal Conductivity	$(Wm^{-1}K^{-1})$
k_m	Thermal Conductivity of Fluid Medium	$(Wm^{-1}K^{-1})$
G	Temperature Gradient	(Km^{-1})
$k_p, k_{particle}$	Thermal Conductivity of the Nanoparticle	$(Wm^{-1}K^{-1})$
ϕ_v	Nanoparticle Volume Concentration	
ϕ'_v	Effective Volume Concentration	
t	Nanolayer Thickness	(m)
β	t/r_o	
γ	$k_{layer}/k_{particle}$	
k_{layer}	Thermal Conductivity of Nanolayer	$(Wm^{-1}K^{-1})$
μ_{nf}	Viscosity of the Nanofluid	$(kgm^{-1}s^{-1})$
μ_{bf}	Viscosity of the Base Fluid	$(kgm^{-1}s^{-1})$
φ	Volume Concentration of Nanofluid	
T	Temperature of Nanofluid	(K)
N_v	Number of Independent Variables	
ε	Arbitrarily Chosen Epsilon Value	
μ_r	μ_{nf}/μ_{bf}	
$L_{x,z}$	Length and Width of Plate	(m)
d	Distance Between Plates	(m)
Δp	Pressure Difference from Inlet to Outlet	(Pa)
G_p	Pressure Gradient	(Pam^{-1})

η	Coefficient of Viscosity	$(kgm^{-1}s^{-1})$
Q	Volumetric Discharge	(m^3s^{-1})
U	Average Velocity	(ms^{-1})
ρ	Density	(kgm^{-3})
Re	Reynolds Number in Microchannel	
$\overrightarrow{v}$	Velocity Vector	(ms^{-1})
$\overline{\overline{\tau}}$	Stress Tensor	$(kgm^{-1}s^{-2})$
I	Unit Tensor	
c_p	Specific Heat Capacity	$(Jkg^{-1}K^{-1})$
p	Local Pressure	(Pa)
T_w	Local Wall Temperature	(K)
T_s	Local Surface Temperature	(K)
T_f	Local Fluid Temperature	(K)
q	Thermal Heat Flux	(Wm^{-2})
q_w	Thermal Heat Flux at Wall	(Wm^{-2})
q_{rad}	Radiated Thermal Heat Transfer	(Wm^{-2})
k_s	Thermal Conductivity of the Solid	$(Wm^{-1}K^{-1})$
Δn	Distance Between Wall Surface and Solid Cell Center	(m)
h_f	Heat Transfer Coefficient	$(Wm^{-2}K^{-1})$
ρ_{eff}	Effective Density of the Nanofluid	(kgm^{-3})
$c_{p,eff}$	Effective Heat Capacity of the Nanofluid	$(Jkg^{-1}K^{-1})$
H_i	Height of Inlet Zone	(m)
W_i	Width of Inlet Zone	(m)
L_i	Length of Inlet Zone	(m)
H_m	Height of Microchannel	(m)
L	Length of Microchannel	(m)
H_s	Height of Silicon Chip	(m)
H_o	Height of Outlet Zone	(m)
W_i	Width of Outlet Zone	(m)
L_o	Length of Outlet Zone	(m)
$T_{f,n+1}$	Temperature Fluid Outside Thermal Boundary Layer	(T)
d_{therm}	Thickness of Thermal Layer	(m)
$T_{f,inlet}$	Temperature of Fluid at Inlet Surface	(T)

Appendix A

Appendix

A.1 Overview

The appendix contains the weekly meeting form.

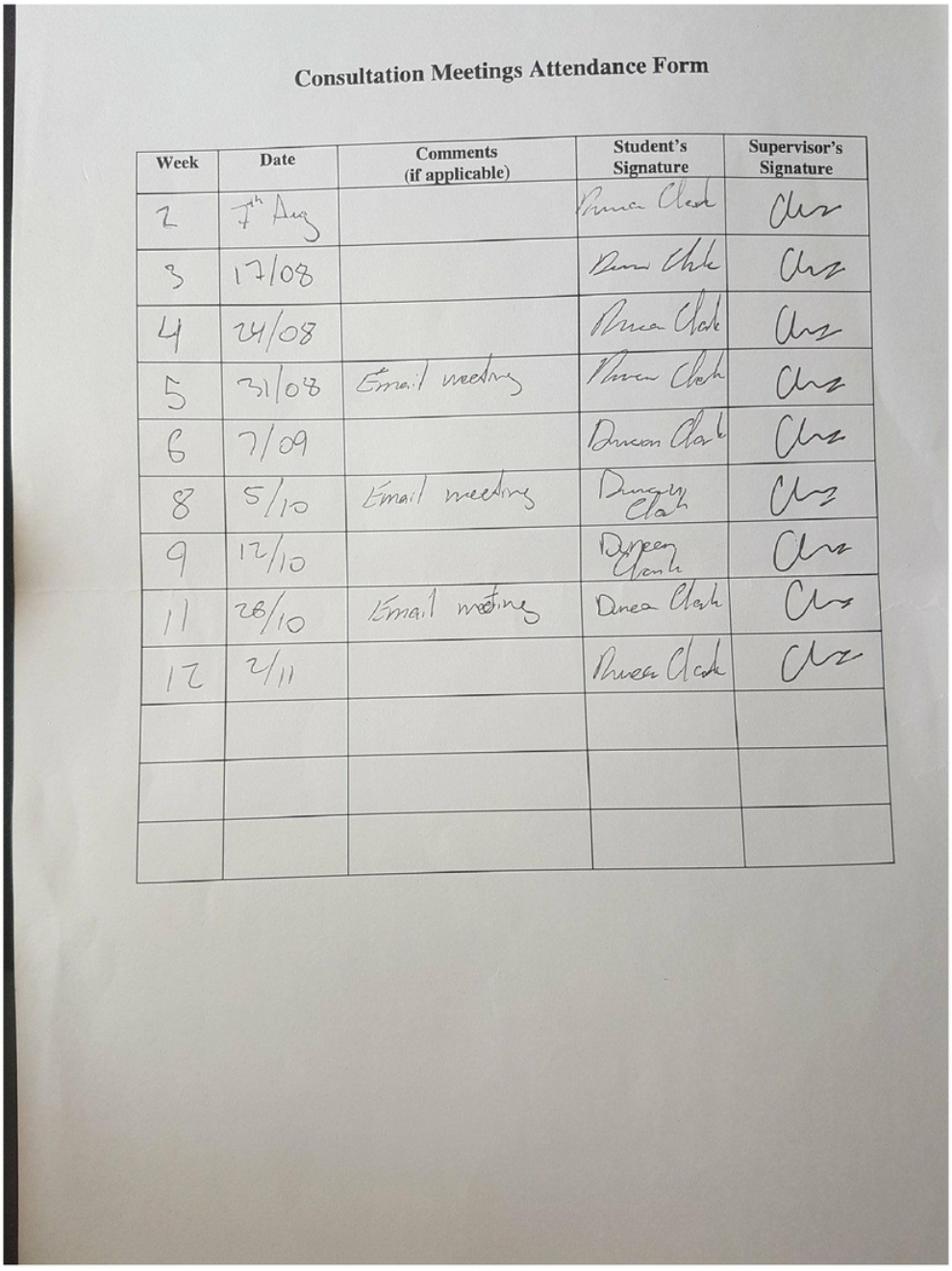

Consultation Meetings Attendance Form

Week	Date	Comments (if applicable)	Student's Signature	Supervisor's Signature
2	1st Aug		Dunea Clark	Chr
3	17/08		Dunea Clark	Chr
4	24/08		Dunea Clark	Chr
5	31/08	Email meeting	Dunea Clark	Chr
6	7/09		Dunea Clark	Chr
8	5/10	Email meeting	Dunea Clark	Chr
9	12/10		Dunea Clark	Chr
11	26/10	Email meeting	Dunea Clark	Chr
12	2/11		Dunea Clark	Chr

Bibliography

[1] W. Yu and S. Choi, "The role of interfacial layers in the enhanced thermal conductivity of nanofluids: A renovated maxwell model," *Journal of Nanoparticle Research*, vol. 5, no. 1/2, pp. 167–171, 2003. [Online]. Available: https://link.springer.com/content/pdf/10.1023%2FA%3A1024438603801.pdf

[2] S. Atashrouz, G. Pazuki, and Y. Alimoradi, "Estimation of the viscosity of nine nanofluids using a hybrid gmdh-type neural network system," *Fluid Phase Equilibria*, vol. 372, pp. 43–48, 2014.

[3] M. Kinnunen, "Examining the limits of moores law: Possible influence of technological convergence on redefining the curriculum in ict institutions," 2015. [Online]. Available: http://file:///C:/Users/43267238/Downloads/Markku.Arimo.Kinnunen-Thesis-Moores-Law-End-2015.pdf

[4] S. Lee, S. U.-S. Choi, S. Li, and J. A. Eastman, "Measuring thermal conductivity of fluids containing oxide nanoparticles," *Journal of Heat Transfer*, vol. 121, no. 2, p. 280, 1999. [Online]. Available: https://www.researchgate.net/publication/236353373_Enhancing_thermal_conductivity_of_fluids_with_nanoparticles

[5] W. Yu, D. M. France, J. L. Routbort, and S. U. S. Choi, "Review and comparison of nanofluid thermal conductivity and heat transfer enhancements," *Heat Transfer Engineering*, vol. 29, no. 5, pp. 432–460, 2008. [Online]. Available: http://www.tandfonline.com/doi/full/10.1080/01457630701850851?scroll=top&needAccess=true&

[6] X. Wang, X. Xu, and S. U. S. Choi, "Thermal conductivity of nanoparticle - fluid mixture," *Journal of Thermophysics and Heat Transfer*, vol. 13, no. 4, pp. 474–480, 1999.

[7] Y. Xuan and W. Roetzel, "Conceptions for heat transfer correlation of nanofluids," *International Journal of Heat and Mass Transfer*, vol. 43, no. 19, pp. 3701–3707, 2000. [Online]. Available: http://www.sciencedirect.com/science/article/pii/S0017931099003695

[8] Y. Xuan and Q. Li, "Heat transfer enhancement of nanofluids," *International Journal of Heat and Fluid Flow*, vol. 21, no. 1, pp. 58–64, 2000. [Online]. Available: http://www.sciencedirect.com/science/article/pii/S0142727X99000673#bBIB3

[9] S. Komarneni, J. Parker, and H. Wollenberger, "Nanophase and nanocomposite materials ii," *MATERIALS RESEARCH SOCIETY*, vol. 457, pp. 16–20, 1996. [Online]. Available: http://www.dtic.mil/dtic/tr/fulltext/u2/a329567.pdf

[10] S. Murshed, K. Leong, and C. Yang, "Enhanced thermal conductivity of tio2water based nanofluids," *International Journal of Thermal Sciences*, vol. 44, no. 4, pp. 367–373, 2005.

[11] M. Corcione, "Empirical correlating equations for predicting the effective thermal conductivity and dynamic viscosity of nanofluids," *Energy Conversion and Management*, vol. 52, no. 1, pp. 789–793, 2011.

[12] R. Prasher, D. Song, J. Wang, and P. Phelan, "Measurements of nanofluid viscosity and its implications for thermal applications," *Applied Physics Letters*, vol. 89, no. 13, p. 133108, 2006.

[13] I. Tavman, A. Turgut, M. Chirtoc, H. Schuchmann, and S. Tavman, "Experimental investigation of viscosity and thermal conductivity of suspensions containing nanosized ceramic particles," *Archives of Materials Science and Engineering*, vol. 34, no. 2, pp. 99–104, 2008. [Online]. Available: https://www.scopus.com/record/display.uri?eid=2-s2.0-77950632748&origin=inward&txGid=32ed52c216475b58fa59bb2a4590092b

[14] B. LotfizadehDehkordi, S. N. Kazi, M. Hamdi, A. Ghadimi, E. Sadeghinezhad, and H. S. C. Metselaar, "Investigation of viscosity and thermal conductivity of alumina nanofluids with addition of sdbs," *Heat and Mass Transfer*, vol. 49, no. 8, pp. 1109–1115, 2013. [Online]. Available: https://link.springer.com/article/10.1007%2Fs00231-013-1153-8

[15] C. Nguyen, F. Desgranges, G. Roy, N. Galanis, T. Mar, S. Boucher, and H. Angue Mintsa, "Temperature and particle-size dependent viscosity data for water-based nanofluids hysteresis phenomenon," *International Journal of Heat and Fluid Flow*, vol. 28, no. 6, pp. 1492–1506, 2007. [Online]. Available: http://www.sciencedirect.com/science/article/pii/S0142727X07000203?via%3Dihub

[16] A. Einstein, "Eine neue bestimmung der molekldimensionen," *Annalen der Physik*, vol. 324, no. 2, pp. 289–306, 1906. [Online]. Available: http://onlinelibrary.wiley.com/doi/10.1002/andp.19063240204/abstract;jsessionid=CCE893D3C9AC711BA96CF85ABB4119CC.f02t04

[17] N. Sait, "Concentration dependence of the viscosity of high polymer solutions. i," *Journal of the Physical Society of Japan*, vol. 5, no. 1, pp. 4–8, 1950. [Online]. Available: http://journals.jps.jp/doi/10.1143/JPSJ.5.4

[18] T. S. Lundgren, "Slow flow through stationary random beds and suspensions of spheres," *Journal of Fluid Mechanics*, vol. 51, no. 02, 1972. [Online].

Available: https://www.cambridge.org/core/journals/journal-of-fluid-mechanics/article/slow-flow-through-stationary-random-beds-and-suspensions-of-spheres/0EE5CC18C12DCE62EC38A85984F428F5

[19] A. G. Ivakhnenko, "Polynomial theory of complex systems," *IEEE Transactions on Systems, Man, and Cybernetics*, vol. SMC-1, no. 4, pp. 364–378, 1971. [Online]. Available: http://ieeexplore.ieee.org/document/4308320/?reload=true

[20] T. Peters, "Physics of continuous matter: Exotic and everyday phenomena in the macroscopic world, 2nd ed., by b. lautrup," *Contemporary Physics*, vol. 54, no. 1, pp. 60–60, 2013. [Online]. Available: http://www.cns.gatech.edu/PHYS-4421/lautrup/book/exact.pdf

[21] A. Lee, D. D. Li, G. E. Lau, and G. H. Yeoh, *Thermal Performance of Nanofluids in Microchannel Equipped with a Synthetic Jet Actuator*. IHTC-15, 2014, pp. 1–15.

[22] W. Anderson and D. L. Bonhaus, "An implicit upwind algorithm for computing turbulent flows on unstructured grids," *Computers and Fluids*, vol. 23, no. 1, pp. 1–21, 1994.

[23] N. Oreskes, K. Shrader-Frechette, and K. Belitz, "Verification, validation, and confirmation of numerical models in the earth sciences," *Science*, vol. 263, no. 5147, pp. 641–646, 1994. [Online]. Available: http://www.jstor.org/stable/pdf/2883078.pdf